



Fermi National Accelerator Laboratory

FERMILAB-Pub-99/341-T

**Long-Baseline Study of the Leading Neutrino Oscillation at a
Neutrino Factory**

V. Barger et al.

*Department of Physics, University of Wisconsin
Madison, Wisconsin 63706, USA*

*Fermi National Accelerator Laboratory
P.O. Box 500, Batavia, Illinois 60510*

December 1999

Submitted to *Physical Review D*

Disclaimer

This report was prepared as an account of work sponsored by an agency of the United States Government. Neither the United States Government nor any agency thereof, nor any of their employees, makes any warranty, expressed or implied, or assumes any legal liability or responsibility for the accuracy, completeness, or usefulness of any information, apparatus, product, or process disclosed, or represents that its use would not infringe privately owned rights. Reference herein to any specific commercial product, process, or service by trade name, trademark, manufacturer, or otherwise, does not necessarily constitute or imply its endorsement, recommendation, or favoring by the United States Government or any agency thereof. The views and opinions of authors expressed herein do not necessarily state or reflect those of the United States Government or any agency thereof.

Distribution

Approved for public release; further dissemination unlimited.

Copyright Notification

This manuscript has been authored by Universities Research Association, Inc. under contract No. DE-AC02-76CH03000 with the U.S. Department of Energy. The United States Government and the publisher, by accepting the article for publication, acknowledges that the United States Government retains a nonexclusive, paid-up, irrevocable, worldwide license to publish or reproduce the published form of this manuscript, or allow others to do so, for United States Government Purposes.

MADPH-99-1145
Fermilab-PUB 99-341-T
AMES-HET 99-12
hep-ph/9911524
November 1999

Long-Baseline Study of the Leading Neutrino Oscillation at a Neutrino Factory

V. Barger¹, S. Geer², R. Raja², and K. Whisnant³

¹*Department of Physics, University of Wisconsin, Madison, WI 53706, USA*

²*Fermi National Accelerator Laboratory, P.O. Box 500, Batavia, IL 60510, USA*

³*Department of Physics and Astronomy, Iowa State University, Ames, IA 50011, USA*

Abstract

Within the framework of three-flavor neutrino oscillations, we consider the physics potential of $\nu_e \rightarrow \nu_\mu$ appearance and $\nu_\mu \rightarrow \nu_\mu$ survival measurements at a neutrino factory for a leading oscillation scale $\delta m^2 \sim 3.5 \times 10^{-3} \text{ eV}^2$. Event rates are evaluated versus baseline and stored muon energy, and optimal values discussed. Over a sizeable region of oscillation parameter space, matter effects would enable the sign of δm^2 to be determined from a comparison of $\nu_e \rightarrow \nu_\mu$ with $\bar{\nu}_e \rightarrow \bar{\nu}_\mu$ event rates and energy distributions. It is important, therefore, that both positive and negative muons can be stored in the ring. Measurements of the $\nu_\mu \rightarrow \nu_\mu$ survival spectrum could determine the magnitude of δm^2 and the leading oscillation amplitude with a precision of $\mathcal{O}(1\%-2\%)$.

I. INTRODUCTION

The SuperKamiokande (SuperK) collaboration [1] has published evidence that muon neutrinos, produced in the earth's atmosphere by cosmic rays, oscillate into other neutrino flavors. The ν_μ survival probability in vacuum for neutrinos of energy E_ν (GeV) traversing a distance L (km) is given by:

$$P(\nu_\mu \rightarrow \nu_\mu) = \sin^2 2\theta_{\text{ATM}} \sin^2(1.267\delta m_{\text{ATM}}^2 L/E_\nu). \quad (1)$$

The SuperK results for the oscillation amplitude $\sin^2 2\theta_{\text{ATM}}$ and the oscillation scale δm_{ATM}^2 are in accord with results obtained from other experiments [2]. From the zenith angle distribution of the muon events, which is related to the distribution in L/E_ν , the mass-squared difference scale of the oscillations was inferred to be [1,3]

$$\delta m_{\text{ATM}}^2 = (3.5_{-2.0}^{+3.5}) \times 10^{-3} \text{ eV}^2 \quad (2)$$

and the amplitude of the oscillations was found to be maximal or nearly maximal,

$$\sin^2 2\theta_{\text{ATM}} = 1_{-0.2}^{+0}. \quad (3)$$

No zenith angle dependence was observed by SuperK for electron events, so it is concluded that electron-neutrinos do not undergo appreciable oscillations at the δm_{ATM}^2 scale of Eq. (2) and that the muon-neutrinos oscillate dominantly to some neutrino flavor other than electron-neutrinos. This interpretation is consistent with the stringent lower limits on the electron-neutrino survival probability $P(\bar{\nu}_e \rightarrow \bar{\nu}_e)$ from the CHOOZ reactor neutrino experiment [4]. Thus it is inferred that atmospheric muon-neutrinos oscillate to tau-neutrinos or to a new sterile neutrino species that has no Standard Model interactions. In the latter case, matter effects would be expected to distort the zenith angle distributions at large zenith angles. The SuperK data presently disfavor muon-neutrino oscillations to sterile neutrinos by two standard deviations [1].

For δm^2 given by Eq. (2), the first minimum in the survival probability occurs at

$$L/E_\nu \simeq 350_{-170}^{+480} \text{ km/GeV}. \quad (4)$$

The detector averaged $P(\nu_\mu \rightarrow \nu_\mu)$ measurement by SuperK does not resolve this minimum because of the smearing over L and inferred E_ν values. Accelerator-based experiments are thus essential to establish the existence of the minimum in the survival probability. The K2K [5] experiment from KEK to SuperK, already underway, has $L = 250$ km and average neutrino energy $\langle E_\nu \rangle = 1.4$ GeV, with an L/E_ν range of 125–250 km/GeV. The MINOS [6] experiment from Fermilab to Soudan has a baseline $L = 732$ km and 3 beam options with $\langle E_\nu \rangle = 3, 6$ and 12 GeV, giving $L/E_\nu = 50$ –250 km/GeV. Other experiments from CERN to detectors in Gran Sasso with a baseline $L = 743$ km are in the final design stages. The energy dependence of the charged-current rate, the neutral-current rate, and τ -appearance with higher energy beams will test the neutrino oscillation hypothesis. The value of δm^2 will be measured in these long-baseline experiments to higher precision than possible with atmospheric neutrinos. For example, MINOS may ultimately be able [7] to make a 10% determination of δm^2 .

Thus the next generation of accelerator long-baseline neutrino experiments are expected to firmly establish neutrino oscillations and improve our knowledge of δm^2 . However, the dominant flux components in these accelerator experiments are ν_μ and $\bar{\nu}_\mu$. To make further progress in determining all of the parameters describing the oscillations it is desirable to also have ν_e and $\bar{\nu}_e$ beams, in addition to beams of higher intensity. With this in mind, it has been pointed out [8,9] that if an intense muon source of the type being developed for a possible future muon collider [10] is used together with a muon storage ring having long straight sections, the resulting “neutrino factory” would produce intense beams containing ν_e ($\bar{\nu}_e$) as well as $\bar{\nu}_\mu$ (ν_μ). In the original neutrino factory proposal [9] it was shown that if the storage ring was tilted down at a large angle, the neutrino beams would be sufficiently intense to produce thousands of interactions in a reasonable sized detector on the other side of the Earth. Neutrino factories have caught the attention of the community, and several groups are developing the concept with BNL, CERN, FNAL, and KEK all being considered as possible sites [11–13].

In Ref. [14] we explored long-baseline neutrino physics at a neutrino factory within the framework of two-flavor oscillations. In the present paper we extend our analysis of the physics potential at neutrino factories, presenting results within the framework of three-flavor oscillations. In particular we discuss: (i) the precise determination of δm_{ATM}^2 ($\sim 1\% - 2\%$) from the measured $\nu_\mu \rightarrow \nu_\mu$ survival probability; (ii) a proof that the sign of δm_{ATM}^2 can in principle be extracted from $\nu_e \rightarrow \nu_\mu$ and $\nu_\mu \rightarrow \nu_e$ appearance measurements by exploiting matter effects that modify these oscillation probabilities; and (iii) the optimal L/E and methodology for the measurements. Table I summarizes the baselines, average electron density in the earth, and the dip angle for various possibilities. Our present analysis focuses on long-baseline experiments with $L = 732$ km (Fermilab \rightarrow Soudan), $L = 2800$ km and 2900 km (Note: Fermilab \rightarrow SLAC ~ 2900 km, Fermilab \rightarrow Seattle, Washington ~ 2700 km), and $L = 7332$ km (Fermilab \rightarrow Gran Sasso).

II. LEADING NEUTRINO OSCILLATION

There are experimental indications of neutrino oscillation effects from the LSND accelerator experiment [15], from the atmospheric neutrino anomaly [1,2,16], and from the solar neutrino deficit [17,18]. Three neutrino mass-squared differences are required to completely explain all these phenomena. However, three neutrinos provide only two distinct δm^2 scales. Therefore, a sterile neutrino must be invoked if all the experimental indications are real. Since the significance of the LSND effect is not at the discovery level, a common approach is to set this anomaly aside until it is confirmed or rejected by the forthcoming Fermilab Mini-BooNE experiment [19] and analyze the solar and atmospheric neutrino deficits within the framework of three-neutrino oscillations. This is the route followed in the present analysis. Thus we take the atmospheric δm^2 scale to be the leading oscillation.

With three neutrinos, the flavor eigenstates ν_α ($\alpha = e, \mu, \tau$) are related to the mass eigenstates ν_j ($j = 1, 2, 3$) in vacuum by

$$\nu_\alpha = \sum_j U_{\alpha j} \nu_j, \quad (5)$$

where U is the unitary Maki-Nakagawa-Sakata (MNS) mixing matrix [20]. We parametrize U by

$$U = \begin{pmatrix} c_{13}c_{12} & c_{13}s_{12} & s_{13}e^{-i\delta} \\ -c_{23}s_{12} - s_{13}s_{23}c_{12}e^{i\delta} & c_{23}c_{12} - s_{13}s_{23}s_{12}e^{i\delta} & c_{13}s_{23} \\ s_{23}s_{12} - s_{13}c_{23}c_{12}e^{i\delta} & -s_{23}c_{12} - s_{13}c_{23}s_{12}e^{i\delta} & c_{13}c_{23} \end{pmatrix}, \quad (6)$$

where $c_{jk} \equiv \cos \theta_{jk}$ and $s_{jk} \equiv \sin \theta_{jk}$. For Majorana neutrinos, U contains two further multiplicative phase factors that modify diagonal entries of U , but these do not enter in oscillation phenomena.

The importance of forward scattering of neutrinos on electrons in the propagation of neutrinos through matter was first pointed out in Ref. [21]. The existence of resonance effects in propagation of neutrinos through the earth in a constant density approximation was then discovered in Ref. [22]. Corrections to the magnitude and sign of the coherent amplitude given by Ref. [21] were made in Refs. [22,23]. The effects of matter are prominent in neutrino oscillation solutions [24] to the solar neutrino anomaly [17,18]. Early calculations for long-baseline experiments were presented in Ref. [25]. Many long-baseline analytical and numerical studies have subsequently been made that include various refinements [26–32].

The propagation of three neutrinos through matter is described by the evolution equation

$$i \frac{d\nu_\alpha}{dx} = \sum_\beta \left[\left(\sum_j U_{\alpha j} U_{\beta j}^* \frac{m_j^2}{2E_\nu} \right) + \frac{A}{2E_\nu} \delta_{\alpha e} \delta_{\beta e} \right] \nu_\beta, \quad (7)$$

where $x = ct$ and $A/(2E_\nu)$ is the amplitude for coherent forward charged-current scattering of ν_e on electrons,

$$A = 2\sqrt{2}G_F Y_e \rho E_\nu = 1.52 \times 10^{-4} \text{ eV}^2 Y_e \rho (\text{g/cm}^3) E (\text{GeV}). \quad (8)$$

Here $Y_e(x)$ is the electron fraction and $\rho(x)$ is the matter density. For neutrino trajectories that pass through the earth's crust, the average density is typically of order 3 gm/cm^3 and $Y_e \simeq 0.5$. The propagation Eq. (7) can be re-expressed in terms of mass-squared differences as

$$i \frac{d\nu_\alpha}{dx} = \sum_\beta \frac{1}{2E_\nu} \left[\delta m_{31}^2 U_{\alpha 3} U_{\beta 3}^* + \delta m_{21}^2 U_{\alpha 2} U_{\beta 2}^* + A \delta_{\alpha e} \delta_{\beta e} \right] \nu_\beta. \quad (9)$$

This evolution equation can be solved numerically for given input values of the δm^2 and mixing matrix elements.

In our analysis we obtain numerical solutions of Eq. (9) for three-neutrino oscillations taking into account the dependence of the density on depth using the Preliminary Reference Earth Model [33]. However, it is instructive to first consider an approximate analytic solution [30] based on the δm^2 hierarchy

$$|\delta m_{32}|^2 \simeq |\delta m_{31}|^2 \gg |\delta m_{21}|^2. \quad (10)$$

implied by oscillation solutions to the atmospheric and solar neutrino anomalies. Then, for short enough distances, the δm_{21}^2 term in Eq. (9) can be dropped and the other two δm^2 set equal,

$$\delta m_{32}^2 = \delta m_{31}^2 \equiv \delta m^2. \quad (11)$$

The evolution equations are then

$$i \frac{d}{dt} \begin{pmatrix} \nu_e \\ \nu_\mu \\ \nu_\tau \end{pmatrix} = \frac{\delta m^2}{2E} \begin{pmatrix} \frac{A}{\delta m^2} + |U_{e3}|^2 & U_{e3}U_{\mu 3}^* & U_{e3}U_{\tau 3}^* \\ U_{e3}^*U_{\mu 3} & |U_{\mu 3}|^2 & U_{\mu 3}U_{\tau 3}^* \\ U_{e3}^*U_{\tau 3} & U_{\mu 3}^*U_{\tau 3} & |U_{\tau 3}|^2 \end{pmatrix} \begin{pmatrix} \nu_e \\ \nu_\mu \\ \nu_\tau \end{pmatrix}. \quad (12)$$

The propagation matrix has eigenvalues

$$\lambda_1 = 0, \quad \lambda_2 = \frac{\delta m^2}{4E} \left[1 + \frac{A}{\delta m^2} - S \right], \quad \lambda_3 = \frac{\delta m^2}{4E} \left[1 + \frac{A}{\delta m^2} + S \right], \quad (13)$$

where

$$S \equiv \sqrt{\left(\frac{A}{\delta m^2} - \cos 2\theta_{13} \right)^2 + \sin^2 2\theta_{13}}. \quad (14)$$

For propagation through matter of constant density, the flavor eigenstates are related to the mass eigenstates ν_j^m by

$$\nu_\alpha = \sum U_{\alpha j}^m \nu_j^m, \quad (15)$$

where

$$U^m = \begin{pmatrix} 0 & c_{13}^m & s_{13}^m \\ -c_{23} & -s_{13}^m s_{23} & c_{13}^m s_{23} \\ s_{23} & -s_{13}^m c_{23} & c_{13}^m c_{23} \end{pmatrix} \quad (16)$$

and θ_{13}^m is related to θ_{13} by

$$\tan 2\theta_{13}^m = \frac{\sin \theta_{13}}{\cos 2\theta_{13} - \frac{A}{\delta m^2}}. \quad (17)$$

We note that U^m has the form of the vacuum U with the substitutions

$$\theta_{13} \rightarrow \theta_{13}^m, \quad \theta_{12} \rightarrow \pi/2, \quad \delta = 0. \quad (18)$$

There are only two mixing angles because the oscillations associated with the solar scale (δm_{21}^2) have not yet developed. The effective phase angle δ vanishes, so CP violation is not possible in the leading oscillation, even after matter effects are included [34]. Equation (17) implies that

$$\sin^2 2\theta_{13}^m = \frac{\sin^2 2\theta_{13}}{\left(\frac{A}{\delta m^2} - \cos 2\theta_{13} \right)^2 + \sin^2 2\theta_{13}}. \quad (19)$$

Thus there is a resonant enhancement for

$$A = \delta m^2 \cos 2\theta_{13} \quad (20)$$

or equivalently

$$E_\nu \approx 15 \text{ GeV} \left(\frac{\delta m^2}{3.5 \times 10^{-3} \text{ eV}^2} \right) \left(\frac{1.5 \text{ g/cm}^3}{\rho Y_e} \right) \cos 2\theta_{13}. \quad (21)$$

The resonance occurs only for positive δm^2 . For negative δm^2 the oscillation amplitude in (19) is smaller than the vacuum oscillation amplitude. Thus the matter effects give us a way in principle to determine the sign of δm^2 .

For a constant Earth density profile, the transition probabilities for a given neutrino flavor are given by

$$P(\nu_\alpha \rightarrow \nu_\beta) = -4 \sum_{j < k} U_{\alpha j}^m U_{\alpha k}^m U_{\beta j}^m U_{\beta k}^m \sin^2 \Delta_{kj}^m, \quad (22)$$

where

$$\Delta_{kj}^m = L(\lambda_k - \lambda_j)/2 \quad (23)$$

and the λ_j are the eigenvalues of the neutrino matrix in Eq. (13). The transition probabilities in the leading oscillation approximation are

$$\begin{aligned} P(\nu_e \rightarrow \nu_\mu) &= s_{23}^2 \sin^2 2\theta_{13}^m \sin^2 \Delta_{32}^m, \\ P(\nu_e \rightarrow \nu_\tau) &= c_{23}^2 \sin^2 2\theta_{13}^m \sin^2 \Delta_{32}^m, \\ P(\nu_\mu \rightarrow \nu_\tau) &= \sin^2 2\theta_{23} \left[(\cos \theta_{13}^m)^2 \sin^2 \Delta_{21}^m + (\sin \theta_{13}^m)^2 \sin^2 \Delta_{31}^m - (\sin \theta_{13}^m \cos \theta_{13}^m)^2 \sin^2 \Delta_{32}^m \right]. \end{aligned} \quad (24)$$

Here the oscillation arguments are

$$\Delta_{32}^m = \Delta_0 S, \quad \Delta_{31}^m = \Delta_0 \frac{1}{2} \left[1 + \frac{A}{\delta m^2} + S \right], \quad \Delta_{21}^m = \Delta_0 \frac{1}{2} \left[1 + \frac{A}{\delta m^2} - S \right], \quad (25)$$

where S is given by Eq. (14) and

$$\Delta_0 = \frac{\delta m_{32}^2 L}{4E} = 1.267 \frac{\delta m_{32}^2 (\text{eV}^2) L (\text{km})}{E_\nu (\text{GeV})}. \quad (26)$$

The Δ_{21}^m term in $P(\nu_\mu \rightarrow \nu_\tau)$ must be retained here because it is not necessarily negligible compared to Δ_{31}^m , due to matter effects. From Eqs. (19), (24) and (25), we see in the limit $\theta_{13} \rightarrow 0$ that $\theta_{13}^m \rightarrow 0$ and the ν_e transition probabilities vanish. We see from Eq. (24) that matter effects are possible for $\nu_\mu \rightarrow \nu_\tau$ oscillations in a three neutrino model. However, these matter effects disappear in the $\theta_{13} = 0$ limit, where

$$S = \left| 1 - \frac{A}{\delta m_{\text{ATM}}^2} \right|, \quad (27)$$

and

$$P(\nu_\mu \rightarrow \nu_\tau) = \sin^2 2\theta_{23} \sin^2(\Delta_0). \quad (28)$$

To have substantial τ event rates from $\nu_\mu \rightarrow \nu_\tau$ oscillations requires high energy neutrino beams because of the kinematic suppression of the τ production cross section near threshold. The $\nu_e \rightarrow \nu_\mu$ and $\nu_\mu \rightarrow \nu_\mu$ oscillation probabilities can be studied with either low or high energy beams and we focus our attention on them in the rest of this paper. A non-zero value of θ_{13} is essential for the occurrence of these oscillations and for the observation of matter effects.

III. NEUTRINO FLUXES AND CROSS-SECTIONS

The distribution $n(x, \Omega) = d^2N/dxd\Omega$ of neutrinos from the decays of an ensemble of polarized negatively-charged muons is given by

$$n_{\nu_\mu}(x, \Omega) = \frac{2x^2}{4\pi} [(3 - 2x) + (1 - 2x)P_\mu \cos \theta] , \quad (29)$$

$$n_{\bar{\nu}_e}(x, \Omega) = \frac{12x^2}{4\pi} [(1 - x) + (1 - x)P_\mu \cos \theta] , \quad (30)$$

where $x \equiv 2E_\nu/m_\mu$, θ is the angle between the neutrino momentum vector and the muon spin direction and P_μ is the average muon polarization along the beam direction. The corresponding distributions for $\bar{\nu}_\mu$ and ν_e from $\mu^+ \rightarrow e^+\bar{\nu}_\mu\nu_e$ are obtained by the replacement $P_{\mu^-} \rightarrow -P_{\mu^+}$ in Eqs. (29) and (30). Only neutrinos emitted in the extreme forward direction ($\cos \theta \simeq 1$) are relevant to the neutrino flux for long-baseline experiments; in this limit

$$E_\nu = xE_\mu . \quad (31)$$

The flux at a distance L from the storage ring can be approximated by

$$\Phi \simeq \frac{n_0\gamma^2}{\pi L^2} , \quad (32)$$

where $\gamma = E_\mu/m_\mu$ and n_0 is the number of neutrinos (or antineutrinos) in a given beam. The charged-current (CC) interaction cross-sections in the detector grow approximately linearly with the neutrino energy

$$\sigma_{\nu N} \simeq 0.67 \times 10^{-38} \text{ cm}^2 \times E_\nu \text{ (GeV)} . \quad (33)$$

$$\sigma_{\bar{\nu} N} \simeq 0.34 \times 10^{-38} \text{ cm}^2 \times E_{\bar{\nu}} \text{ (GeV)} . \quad (34)$$

Thus, the event rates in the absence of oscillations are

$$N \sim (E_\mu)^3/L^2 . \quad (35)$$

The ν_μ ($\bar{\nu}_\mu$) event energies peak at the stored μ^- (μ^+) energy while the $\bar{\nu}_e$ (ν_e) energies peak at about 3/4 of the stored μ^- (μ^+) energy. The lepton spectra from the charged-current interactions can be obtained by folding the event rates with the $d\sigma/dy$ distributions, where $y = 1 - E_\ell/E_\nu$.

For no oscillations, the average observed neutrino energies would be

$$\langle E_{\nu_\mu} \rangle = 0.7E_{\mu^-} , \quad (36)$$

$$\langle E_{\bar{\nu}_e} \rangle = 0.6E_{\mu^-} . \quad (37)$$

Thus, from Eq. (4), the first maximum in the leading oscillation occurs for

$$L/E_\mu \sim 230_{-110}^{+310} \text{ km/GeV} . \quad (38)$$

For maximal oscillation effects the baseline and stored energy should be chosen to satisfy Eq. (38). In order to have sufficient event rates at > 1000 km distances, the lowest practical muon energy is about 10 GeV. The corresponding L from Eq. (38) is close to the 2900 km baseline from Fermilab to SLAC.

IV. OSCILLATION CHANNELS

The decays of stored muons along the straight sections of the storage ring give well-collimated neutrino beams of specified flavor composition. For stored μ^- , the $\mu^- \rightarrow \nu_\mu \bar{\nu}_e e^-$ decays give ν_μ and $\bar{\nu}_e$ beams with the known energy distributions given by Eq. (29) (see Fig. 4 of [14]). In this paper we restrict our attention to detection of muons. The relevant oscillation signatures for stored μ^- are given in Table II. Corresponding signatures for stored μ^+ are obtained by the interchange $\nu \leftrightarrow \bar{\nu}$ and changing the signs of the electric charges of the leptons.

The oscillations to ν_τ feed the same final state as oscillations to ν_μ through the decays $\tau \rightarrow \mu$ of the produced τ -leptons. Thus detection of muons determines linear combinations of oscillation probabilities

$$N(\mu^-) = \langle \Phi P(\nu_\mu \rightarrow \nu_\mu) \sigma(\nu_\mu \rightarrow \mu^-) \rangle + \langle \Phi P(\nu_\mu \rightarrow \nu_\tau) \sigma(\nu_\tau \rightarrow \tau^-) \rangle \text{BF}(\tau^- \rightarrow \mu^-), \quad (39)$$

$$N(\mu^+) = \langle \Phi P(\bar{\nu}_e \rightarrow \bar{\nu}_\mu) \sigma(\bar{\nu}_\mu \rightarrow \mu^+) \rangle + \langle \Phi P(\bar{\nu}_e \rightarrow \bar{\nu}_\tau) \sigma(\bar{\nu}_\tau \rightarrow \tau^+) \rangle \text{BF}(\tau^+ \rightarrow \mu^+), \quad (40)$$

where Φ is the flux and $\langle \rangle$ denotes a spectrum average and integration over final state energies. Neglecting the small matter effects in $\nu_\mu \rightarrow \nu_\tau$, the leading oscillation rates from Eqs. (24) and (28) would be

$$N(\mu^-) = \langle \Phi [1 - s_{23}^2 \sin^2 2\theta_{13}^m \sin^2 \Delta_{32}^m - \sin^2 2\theta_{23} \sin^2 \Delta_0] \sigma(\nu_\mu \rightarrow \mu^-) \rangle + \sin^2 2\theta_{23} \langle \Phi \sin^2 \Delta_{32} \sigma(\nu_\tau \rightarrow \tau^-) \rangle \text{BF}(\tau^- \rightarrow \mu^-), \quad (41)$$

$$N(\mu^+) = s_{23}^2 \sin^2 2\theta_{13}^m \langle \Phi \sin^2 \Delta_{32}^m \sigma(\bar{\nu}_\mu \rightarrow \mu^+) \rangle + c_{23}^2 \sin^2 2\theta_{13}^m \langle \Phi \sin^2 \Delta_{32}^m \sigma(\bar{\nu}_\tau \rightarrow \tau^+) \rangle \text{BF}(\tau^+ \rightarrow \mu^+). \quad (42)$$

The τ -contributions will be suppressed at low stored muon energies (~ 10 GeV) by the kinematic suppression of the tau cross section near the threshold for tau production. The tau neutrino interactions can be identified by (i) kinematics (p_T relative to the neutrino beam direction and the y -distribution of the decay muon), or (ii) direct evidence for $\tau \rightarrow 1$ -prong or $\tau \rightarrow 3$ -prong decays by detecting kinks or displaced vertices in, for example, emulsion detectors, or by imaging Cherenkov rings that the tau generates in C_6F_{14} liquid [35]. Henceforth we concentrate our analysis strictly on primary muons from ν_μ under the assumption that the contributions of muons from tau decay can be resolved.

V. PREDICTED NEUTRINO OSCILLATION EVENT RATES

For a quantitative analysis of neutrino oscillation event rates in long-baseline experiments, we begin with the following set of oscillation parameters:

$$\begin{aligned} |\delta m_{32}^2| &= 3.5 \times 10^{-3} \text{ eV}^2 \\ |\delta m_{21}^2| &= 5 \times 10^{-5} \text{ eV}^2 \\ s_{13} &= 0.10 \quad (\sin^2 2\theta_{13} = 0.04) \\ s_{23} &= 0.71 \quad (\sin^2 2\theta_{23} = 1.00) \\ s_{12} &= 0.53 \quad (\sin^2 2\theta_{12} = 0.80) \\ \delta &= 0 \end{aligned} \quad (43)$$

The values of δm_{32}^2 and s_{23} govern the atmospheric neutrino oscillations. The values of δm_{21}^2 and s_{12} control the solar neutrino oscillations. We select the large-angle matter solution [36] because it is the most optimistic choice for obtaining any effects in long-baseline experiments from the subleading δm_{21}^2 scale. The value of s_{13} determines the size of the matter effects for the leading oscillations. The value of δm_{31}^2 is determined from δm_{32}^2 and δm_{21}^2 by the sum rule

$$\delta m_{31}^2 = \delta m_{32}^2 + \delta m_{21}^2. \quad (44)$$

The subleading oscillation effects associated with the δm_{21}^2 in Eq. (43) are usually small in comparison with the leading oscillation, so either of the other two solar solution possibilities (small angle matter or large-angle vacuum oscillations) would lead to results similar to the representative case above; we will remark below when the subleading oscillation effects are appreciable. The long-baseline oscillations are controlled by the three parameters δm_{32}^2 , s_{23} and s_{13} . The matter effects in the leading oscillation are critically dependent on s_{13} .

We calculate neutrino event rates, with and without oscillations, for a neutrino factory with 2×10^{20} stored muons/year and a 10 kiloton detector. For the neutrino flux, energy distributions and cross sections we use Eqs. (29)–(34). The oscillation probabilities are calculated by integrating Eq. (7) numerically from the source to the detector using a Runge–Kutta method, and averaging over the neutrino energy distribution. For the Earth’s density we use the results of the Preliminary Reference Earth Model [33]. In these initial exploratory results we neglect the stored muon beam momentum-spread and angular-divergence, which we later incorporate in Sec. VI. Fig. 1a shows the event rates at $L = 732$ km versus stored muon (or antimuon) energy E_μ for the oscillation parameters in Eq. (43). We show in Fig. 1b the corresponding event rates with $\delta m_{21}^2 \sim 10^{-10}$ eV² for the subleading oscillation scale, i.e., appropriate for vacuum long-wavelength solar oscillations. We note the following:

- (i) For the appearance channels $\nu_e \rightarrow \nu_\mu$ and $\bar{\nu}_e \rightarrow \bar{\nu}_\mu$, the main difference in rates comes from the difference in the neutrino and antineutrino cross sections. Matter effects, which arise when the sign of δm_{32}^2 is changed, are seen to be relatively small in Fig. 1b. This is to be expected since the characteristic wavelength for matter effects at these energies is of order the Earth’s diameter, which is much larger than 732 km.
- (ii) The effects of the subleading mass scale, δm_{21}^2 , are evident by comparing the appearance channels in Fig. 1a to those in Fig. 1b. For the large-angle MSW solution, $\delta m_{21}^2 = 5 \times 10^{-5}$ eV², the interplay of the subleading scale with matter and the sign of δm_{32}^2 affects the rates at the 20% level. We have found that this effect increases as $\sin^2 2\theta_{13} \rightarrow 0$, when the subleading leading oscillation, with its larger oscillation amplitude, can begin to compete with the leading oscillation, which has a small amplitude in this limit [37].
- (iii) At lower muon energies (10 GeV or less) the survival probabilities for the $\nu_\mu \rightarrow \nu_\mu$ and $\bar{\nu}_\mu \rightarrow \bar{\nu}_\mu$ channels decrease with decreasing energy, but do not reach their minimum values, on average, for $E_\mu > 5$ GeV.
- (iv) The survival rates do not depend appreciably on the sign of δm_{32}^2 , which means that matter effects are small in these channels at this distance, as is the case for the appearance channels.

In Fig. 2 we show similar results for $L = 2900$ km, from which we conclude:

- (i) The largest event rate suppression in the survival channels occurs at energies $E_\mu \sim 10$ GeV.
- (ii) Changing the sign of δm_{32}^2 causes noticeable changes in the event rates in the appearance channels $\nu_e \rightarrow \nu_\mu$ and $\bar{\nu}_e \rightarrow \bar{\nu}_\mu$. By comparing Fig. 2a with Fig. 2b we see that the subleading oscillation scale has a smaller relative effect for $L = 2900$ km than for $L = 732$ km (Fig. 1), so these changes must largely arise from matter effects.

In Fig. 3 we show similar results for $L = 7332$ km, from which we conclude:

- (i) Matter effects have now grown quite large, as evidenced by the large variation in the appearance event rates in Fig. 3a when the sign of δm_{32}^2 is changed. We have found that the results using the large-angle MSW and vacuum solar scales for the subleading oscillations are nearly identical at this distance.
- (ii) A minimum in the survival probability is clearly visible near $E_\mu = 25$ GeV. Also, the *survival* rates are now sensitive to the sign of δm_{32}^2 for $E_\mu \sim 15 - 25$ GeV, indicating matter effects. Unfortunately, the number of events in one of the appearance channels (either $\nu_e \rightarrow \nu_\mu$ or $\bar{\nu}_e \rightarrow \bar{\nu}_\mu$, depending on the sign of δm_{32}^2) falls below 10 for these energies, even for $\sin^2 2\theta_{13} = 0.04$. In general, the event rates at 7332 km are below those at 2900 km due to a lower flux.
- (iii) By comparing Fig. 3a with Fig. 3b we see that matter effects in the survival channels are drastically reduced as $\sin^2 2\theta_{13}$ is decreased, as predicted in Eq. (28).
- (iv) The number of events in the appearance channels is sufficiently large to allow a determination of the sign of δm_{32}^2 , at least for the $L = 2900$ km and 7332 km distances.

Next we show in Fig. 4a the L dependence of the oscillations at a fixed muon energy of 10 GeV. Here we see that $L \simeq 2900$ km is the first minimum in the survival probability and that $L \simeq 5500$ km corresponds to a maximum in the survival probability; matter effects are sizable for $L \sim 5000 - 8000$ km. In the appearance channels, matter effects turn on as L increases, causing one of the appearance channels to be highly suppressed.

Similar results for $E_\mu = 50$ GeV are shown in Fig. 4b. We see that the appearance event rates scale roughly with E_μ , as expected from the product of the E_μ^3 behavior of the unoscillated rates (Eq. (35)) and the E_ν^{-2} dependence of the oscillatory factor for small oscillation arguments (Eqs. 24–26). The L dependence is relatively flat at low L for the channel that is not suppressed by matter, as expected from the product of the $1/L^2$ behavior of the flux and the L^2 dependence of the oscillatory factor. The survival rates are much higher for 50 GeV than for 10 GeV, but they do not reach a minimum for $L < 10000$ km.

Figures 1–4 assume $|\delta m_{32}^2| = 3.5 \times 10^{-3}$ eV², the favored value from atmospheric measurements from SuperK. Long-baseline experiments should be able to determine $|\delta m_{32}^2|$ with high precision if the event rates associated with oscillations are appreciable. Figure 5 shows the sensitivity of the event rates to changes in δm_{32}^2 for $L = 2900$ km and $E_\mu = 10$ or 50 GeV. At $E_\mu = 10$ GeV the survival probability has a minimum near $|\delta m_{32}^2| = 3.5 \times 10^{-3}$ eV², but

the appearance rates are modest. At $E_\mu = 50$ GeV the appearance rates are much higher, but the survival probability has a minimum only for higher $|\delta m_{32}^2|$. Therefore we see that at $L = 2900$ km, if δm_{32}^2 is close to the value favored by SuperK, there is a trade-off between choosing a relatively low E_μ to optimize the survival probability measurements, or choosing a higher energy to optimize the appearance signal.

Figure 6 shows similar curves for $L = 7332$ km with $E_\mu = 25$ and 50 GeV. At $E_\mu = 25$ GeV the survival probability has a minimum near $|\delta m_{32}^2| = 3.5 \times 10^{-3}$ eV², with appreciable appearance rates for nearby values of δm_{32}^2 , and matter effects are evident for $|\delta m_{32}^2| \geq 3 \times 10^{-3}$ eV². At $E_\mu = 50$ GeV, the appearance rates are higher than for 25 GeV (especially in the matter-suppressed channel) and the disappearance probability is appreciable over a range of $|\delta m_{32}^2|$. However, matter effects in the survival probability are noticeable only for $|\delta m_{32}^2| > 7 \times 10^{-3}$ eV².

Figure 7 shows the minimum value of $\sin^2 2\theta_{13}$ that gives 10 $\nu_e \rightarrow \nu_\mu$ appearance events versus E_μ for $L = 732, 2900,$ and 7332 km, when $\delta m_{21}^2 \sim 10^{-10}$ eV² (the solar vacuum oscillation value). The lower (upper) curves are for matter-enhanced (matter-suppressed) oscillations with $\delta m_{32}^2 > 0$ ($\delta m_{32}^2 < 0$); the corresponding curves for $\bar{\nu}_e \rightarrow \bar{\nu}_\mu$ appearance can be empirically obtained by changing the sign of δm_{32}^2 and multiplying by 2. We see that increased E_μ improves the ability to discover appearance channels, although there are limiting returns for going to very high E_μ . The sensitivity to the matter-suppressed channel is especially weak at longer distances (e.g. $L = 7332$ km in this case). The corresponding curves for the large-angle MSW solar solution (e.g. $\delta m_{21}^2 = 5 \times 10^{-5}$ eV²) are much different for $L = 732$ km, and somewhat different at $L = 2900$ km, due to contamination by the subleading oscillation, as expected from the discussion of Figs. 1 and 2. If large-angle solar oscillations are the correct solution to the solar anomaly, then $L = 7332$ km has the merit that the subleading oscillation does not affect the interpretation of $\nu_e \rightarrow \nu_\mu$ appearance, as it does at $L = 732$ and 2900 km.

As discussed in Sec. II, the leading oscillation approximation leads to a simple expressions for the oscillation argument of the $\nu_e \rightarrow \nu_\mu$ probability (see Eqs. (25) and (27)). Then the $\nu_e \rightarrow \nu_\mu$ appearance event rate can be approximated by

$$N \simeq \langle \Phi P(\nu_e \rightarrow \nu_\mu) \sigma(\nu_\mu \rightarrow \mu^-) \rangle \quad (45)$$

$$\simeq 300 \left(\frac{n_0}{2 \times 10^{20} \mu/\text{yr}} \right) \left(\frac{\text{size}}{10 \text{ kt}} \right) \left(\frac{E_\mu}{10 \text{ GeV}} \right)^3 \left(\frac{7332 \text{ km}}{L} \right)^2 \frac{\langle E_\nu \rangle}{E_\mu} \langle P(\nu_e \rightarrow \nu_\mu) \rangle,$$

where the angle brackets denote averages over neutrino energy, and $\langle E_\nu \rangle = 0.6 E_\mu$. The average probability can be estimated by evaluating the probability at $\langle E_\nu \rangle$ in the small $\sin^2 2\theta_{13}$ limit,

$$\langle P(\nu_e \rightarrow \nu_\mu) \rangle \simeq \frac{\sin^2 2\theta_{13}}{\left| 1 - \frac{\langle A \rangle}{\delta m_{32}^2} \right|^2} \sin^2 \left[1.27 \frac{\delta m_{32}^2 L}{\langle E_\nu \rangle} \left| 1 - \frac{\langle A \rangle}{\delta m_{32}^2} \right| \right], \quad (46)$$

where $\langle A \rangle$ is given by Eq. (8) evaluated at $\langle E_\nu \rangle$. Equation (45) gives reasonably accurate results whenever $\sin^2 2\theta_{13}$ is below 0.01 provided that contributions to the subleading oscillation are not important. Approximate antineutrino rates can be obtained by the substitution $A \rightarrow -A$ in Eq. (46) and by dividing the results of Eq. (45) by 2.

VI. MORE DETAILED SIMULATIONS

To obtain a more realistic calculation of the event rates at a neutrino factory we have simulated a neutrino beam formed by muons decaying along a 1 km long straight-section. In our simulations the muon beam has a momentum spread given by $\sigma_p/p = 0.02$, and horizontal and vertical beam divergences given by $\sigma_\theta = 0.1/\gamma$ where $\gamma = E_\mu/m_\mu$. The finite beam momentum spread and angular divergence modify the event rates at a distant site by a few percent. We have also included in our simulations a parametrization of the detector resolution functions for an iron-scintillator neutrino detector [6,7]. We assume that muon energies can be measured by range with a precision given by $\sigma_E/E = 0.05$. Shower energies are assumed to be measured with precisions given by $\sigma_E/E = 0.53/\sqrt{E}$ if $E > 3$ GeV and $\sigma_E/E = 0.80/\sqrt{E}$ if $E < 3$ GeV with, in both cases, a constant term of 0.07 added in quadrature.

For each of the relevant oscillation channels, the predicted annual CC event samples (from 2×10^{20} muon decays) corresponding to the oscillation parameters of Eq. (43) are shown in Table III for both signs of δm_{32}^2 . The tabulated rates are for a 10 kt detector at baselines of $L = 732$ km, 2800 km, and 7332 km, with $E_\mu = 10, 30$ and 50 GeV. The statistical uncertainties on the calculated event rates from the Monte Carlo simulations are about 2.5%. Consider first the sensitivity of the oscillation signals to matter effects, and hence to the sign of δm_{32}^2 . Note that most of the event rates are insensitive to matter effects. However, the $\nu_e \rightarrow \nu_\mu$ CC rates are significantly modified by matter, and hence a measurement of events with wrong-sign muons can in principle determine the sign of δm_{32}^2 . To illustrate this, consider the $\nu_e \rightarrow \nu_\mu$ CC rates when $L = 2800$ km and $E_\mu = 50$ GeV (30 GeV). If δm_{32}^2 is positive, 894 (486) wrong-sign muon events are expected in a 10 kt-yr data sample. However, if δm_{32}^2 is negative, the corresponding rates are 338 (130) events. Hence, if all the oscillation parameters are known except the sign of δm_{32}^2 , the event rates can be used to determine the sign. The statistical significance of this sign determination improves slowly with increasing E_μ . In practice, the oscillation parameters will not be precisely known. However, the sign of δm_{32}^2 can still be uniquely determined from the wrong-sign muon measurements if both $\nu_e \rightarrow \nu_\mu$ rates (positive stored muons) and $\bar{\nu}_e \rightarrow \bar{\nu}_\mu$ rates (negative stored muons) are determined. For the examples we are considering, if δm_{32}^2 is positive the $\nu_e \rightarrow \nu_\mu$ rates will be larger than the $\bar{\nu}_e \rightarrow \bar{\nu}_\mu$ rates by a factor of a few. In contrast, if δm_{32}^2 is negative the $\nu_e \rightarrow \nu_\mu$ rates will be comparable to, or smaller than, the $\bar{\nu}_e \rightarrow \bar{\nu}_\mu$ rates. There is additional information in the spectrum of CC events producing wrong-sign muons. The predicted measured energy distributions (including detector resolutions), for CC events containing wrong-sign muons are shown as a function of both the magnitude and sign of δm_{32}^2 in Figs. 8 and 9 when, respectively, 30 GeV positive and negative muons are stored in the ring, and $L = 2800$ km. Both the shapes and normalizations of the distributions are sensitive to the sign and magnitude of δm_{32}^2 . In particular if δm_{32}^2 is negative (positive) the μ^- appearance events from $\nu_e \rightarrow \nu_\mu$ oscillations will peak at higher (lower) energies than the μ^+ appearance events from $\bar{\nu}_e \rightarrow \bar{\nu}_\mu$ oscillations. We conclude that if both positive and negative muons can be stored at different times in the neutrino factory, then wrong-sign muon appearance measurements can distinguish the sign of δm_{32}^2 and determine its magnitude.

We next consider a less favorable region of parameter space in which the $\nu_e \rightarrow \nu_\mu$

oscillation amplitude is reduced by a large factor. Table IV presents the event rates when $\sin^2 2\theta_{13}$ is reduced by an order of magnitude ($s_{13} = 0.032$ or $\sin^2 2\theta_{13} = 0.004$) with the other oscillation parameters as in Eq. (43). Returning to our example ($L = 2800$ km, $E_\mu = 50$ GeV) we note that if δm_{32}^2 is positive (negative) we expect 108 (25) wrong-sign CC events per 10 kt-yr when positive muons are stored, and 29 (30) events when negative muons are stored. Hence, in this case we are still above, but close to, the threshold below which a statistically significant determination of the sign of δm_{32}^2 will only be possible with larger data samples. Based on Tables III and IV we can estimate the minimum values of $\sin^2 2\theta_{13}$ (when all of the other parameters are as specified in Eq. (43)) for which (i) we expect a measurable wrong-sign muon signal (10 event sensitivity), and (ii) we can determine the sign of δm_{32}^2 (at 3 standard deviations). Figure 10 summarizes our estimates for these minimum $\sin^2 2\theta_{13}$ versus L and E_μ . Note that to measure a wrong-sign muon signal over the largest $\sin^2 2\theta_{13}$ range, high E_μ and “short” L are preferred. However, if L is too short the unoscillated CC event rates get very large, and hence backgrounds become significant. If the background rates are at the level of 10^{-5} – 10^{-6} of the total CC rates [38], then $L = 2800$ km is probably preferred over 732 km. To be able to determine the sign of δm_{32}^2 over the largest $\sin^2 2\theta_{13}$ range, high E_μ is once again preferred. Since matter effects become small for short L and event statistics become small for very large L , there appears to be an optimal L for determining the sign of δm_{32}^2 . Of the 3 baselines we have considered, $L = 2800$ km is preferred. From these considerations we would conclude that for wrong-sign muon measurements $L = 2800$ km is a good choice for the baseline, and high energy stored muons ($E_\mu = 50$ GeV) are preferred, although we note that decreasing E_μ from 50 GeV to 30 GeV decreases the sensitive $\sin^2 2\theta_{13}$ range by less than a factor of two.

We next turn our attention to muon survival measurements. The $\nu_\mu \rightarrow \nu_\mu$ rates shown in Table III are significantly less than the corresponding rates in the absence of oscillations. As an example, consider $L = 2800$ km with $E_\mu = 10$ GeV and 30 GeV. The predicted measured energy distributions (including detector resolutions) for interacting muon neutrinos are shown for the two energies in Figs. 11 and 12 respectively versus δm_{32}^2 with the other oscillation parameters given by Eq. (43). The shapes and normalizations for the predicted distributions are very different from the expected distribution that would be observed in the absence of oscillations. The shapes of the predicted ν_μ CC interaction distributions are sensitive to the magnitude of δm_{32}^2 . The dip in the predicted rate that corresponds to the first oscillation maximum (when $1.267 \delta m_{32}^2 L / E_\nu = \pi$) can be clearly seen. At the higher E_μ the contribution from poorly measured higher energy ν_μ CC interactions reduces the significance of the dip. To understand the statistical precision with which δm_{32}^2 and $\sin^2 2\theta_{13}$ can be extracted from a fit to the measured ν_μ CC interaction distribution, we have generated Monte Carlo data sets with the appropriate statistics for various values of the oscillation parameters, and fit the resulting simulated distributions. As an example, Figs. 13 and 14 show fit results for $E_\mu = 30$ GeV with $L = 2800$ km and $E_\mu = 50$ GeV with $L = 7332$ km. The precision of the fits for various L and E_μ are summarized in Table V for $\sin^2 2\theta_{23} = 1.0$ and $\delta m_{32}^2 = 0.35 \times 10^2 \text{ eV}^2$. In order to extract the fitted information, we have had to limit the fits to energy ranges where the information is maximally available. It can be seen from Table V that the parameters are ill constrained for the shorter baseline of 732 km. For the 10 GeV ring, $L = 2800$ km and for the 30 or 50 GeV ring $L = 7332$ km seem to be the optimal baseline lengths for maximum precision in $\sin^2 2\theta_{23}$ and δm_{32}^2 .

VII. CONCLUSIONS

Within the framework of three-flavor oscillations, we have explored the sensitivity of muon appearance and muon disappearance measurements at a neutrino factory in which there are 2×10^{20} muon decays per year in a beam-forming straight section that points at a 10 kt detector. Three stored muon energies (10, 30, and 50 GeV) and three baselines (732, 2800, and 7332 km) have been explicitly considered. Our results are summarized in Table VI.

If data can be taken alternately with positive and negative muons stored in the ring, a measurement of the wrong-sign muon appearance rates and spectra can uniquely determine the sign of δm_{32}^2 provided the oscillation amplitude is sufficiently large ($\sin^2 2\theta_{13} > 0.005$ for $L = 2800$ km and $E_\mu = 30$ GeV). Of the three baselines we have considered, $L = 2800$ km is preferred for this measurement since $L = 732$ km is too short (matter effects too small) and $L = 7332$ km is too long (statistics too limited) to obtain good sensitivity to the sign of δm_{32}^2 . The sensitivity to wrong-sign muon appearance, characterized by the minimum $\sin^2 2\theta_{13}$ for which a signal can be detected at the 10 events per year level, improves linearly with E_μ . For $L = 2800$ km and $E_\mu = 30$ GeV the minimum $\sin^2 2\theta_{13} = 0.0007$. This can be improved to $\sin^2 2\theta_{13} = 0.0004$ by either increasing E_μ to 50 GeV, or by increasing the detector mass by a factor of 1.8.

The sensitivity for the survival measurements can be optimized by choosing L and E_μ so that L/E_ν is close to the first minimum in the survival probability. For $L = 2800$ km this corresponds to $E_\mu \sim 10$ GeV. For $\delta m_{32}^2 = 0.0035$ eV²/c⁴ and $\sin^2 2\theta_{23} = 1$ the statistical precision of the resulting δm_{32}^2 and $\sin^2 2\theta_{23}$ measurements based on fitting the observed $\nu_\mu \rightarrow \nu_\mu$ spectra are respectively 2.4% and 1.1%. However, optimization for the appearance channels suggests choosing a higher E_μ . For example, choosing $E_\mu = 30$ GeV the precisions for the δm_{32}^2 and $\sin^2 2\theta_{23}$ measurements become 3.2% and 2.0%. With these levels of statistical precision, systematic effects (for example, the uncertainty on the neutrino flux) may dominate. For the region of three-flavor-mixing parameter space that we have explored, we conclude that $L = 2800$ km with $E_\mu = 30$ GeV would enable the very precise determination of $|\delta m_{32}^2|$ and $\sin^2 2\theta_{23}$ from muon survival, the determination of $\sin^2 2\theta_{13}$ from muon appearance, and the sign of δm_{32}^2 from matter effects (e.g., by comparing $\nu_e \rightarrow \nu_\mu$ with $\bar{\nu}_e \rightarrow \bar{\nu}_\mu$).

Finally, we note that if no appearance signal were observed, the implied very low value of $\sin^2 2\theta_{13}$ might provide a window of opportunity for detecting oscillations driven by the smaller (solar neutrino deficit) scale δm_{21}^2 , should it be the large-angle MSW solution. This requires further study.

ACKNOWLEDGMENTS

We thank S. Parke for discussions. This research was supported in part by the U.S. Department of Energy under Grants No. DE-FG02-94ER40817 and No. DE-FG02-95ER40896 and in part by the University of Wisconsin Research Committee with funds granted by the Wisconsin Alumni Research Foundation. Part of this work was performed at the Fermi National Accelerator Laboratory, which is operated by the Universities Research Association, under contract No. DE-AC02-76CH03000 with the U.S. Department of Energy.

REFERENCES

- [1] Super-Kamiokande Collaboration, Y. Fukuda *et al.*, Phys. Lett. **B433**, 9 (1998); Phys. Lett. **B436**, 33 (1998); Phys. Rev. Lett. **81**, 1562 (1998); Phys. Rev. Lett. **82**, 2644 (1999).
- [2] Kamiokande collaboration, K.S. Hirata *et al.*, Phys. Lett. **B280**, 146 (1992); Y. Fukuda *et al.*, Phys. Lett. **B335**, 237 (1994); IMB collaboration, R. Becker-Szendy *et al.*, Nucl. Phys. Proc. Suppl. **38B**, 331 (1995); Soudan-2 collaboration, W.W.M. Allison *et al.*, Phys. Lett. **B391**, 491 (1997); MACRO collaboration, M. Ambrosio *et al.*, Phys. Lett. **B434**, 451 (1998).
- [3] M.C. Gonzalez-Garcia, hep-ph/9910494; G.L. Fogli, E. Lisi, A. Marrone, and G. Scioscia, Phys. Rev. **D59**, 033001 (1999); V. Barger, T.J. Weiler and K. Whisnant, Phys. Lett. **B440**, 1 (1998); M.C. Gonzalez-Garcia, H. Nunokawa, O.L. Peres, and J.W.F. Valle, Nucl. Phys. **B543**, 3 (1998).
- [4] CHOOZ Collaboration, M. Apollonio *et al.*, Phys. Lett. **B420**, 320 (1998).
- [5] K. Nishikawa *et al.* (KEK-PS E362 Collab.), “Proposal for a Long Baseline Neutrino Oscillation Experiment, using KEK-PS and Super-Kamiokande”, 1995, unpublished; INS-924, April 1992, submitted to J. Phys. Soc. Jap.; Y. Oyama, Proc. of the YITP Workshop on Flavor Physics, Kyoto, Japan, 1998, hep-ex/9803014.
- [6] MINOS Collaboration, “Neutrino Oscillation Physics at Fermilab: The NuMI-MINOS Project,” NuMI-L-375, May 1998.
- [7] D. A. Petyt, “A study of parameter measurement in a long-baseline neutrino oscillation experiment”, Thesis submitted to Univ. of Oxford, England, 1998.
- [8] S. Geer, “Neutrino beams from muon storage rings: characteristics and physics potential”, FERMILAB-PUB-97-389, 1997, presented at the Workshop on Physics at the First Muon Collider and Front-End of a Muon Collider, November, 1997.
- [9] S. Geer, Phys. Rev. **D57**, 6989 (1998).
- [10] C. Ankenbrandt *et al.* (Muon Collider Collaboration), Phys. Rev. ST Accel. Beams **2**, 081001 (1999).
- [11] A. De Rujula, M.B. Gavela, and P. Hernandez, Nucl. Phys. **B547**, 21 (1999).
- [12] M. Campanelli, A. Bueno, and A. Rubbia, hep-ph/9905240.
- [13] R.B. Palmer *et al.* (Muon Collider Collaboration), <http://pubweb/bnl.gov/people/palmer/nu/params.ps>
- [14] V. Barger, S. Geer, and K. Whisnant, hep-ph/9906487, to be published in Phys. Rev. D.
- [15] C. Athanassopoulos *et al.* (LSND Collab.), Phys. Rev. Lett. **77**, 3082 (1996); Phys. Rev. Lett. **81**, 1774 (1998).
- [16] V. Barger and K. Whisnant, Phys. Lett. **209B**, 365 (1988); J.G. Learned, S. Pakvasa, and T.J. Weiler, *ibid.* **207B**, 79 (1988); K. Hidaka, M. Honda, and S. Midorikawa, Phys. Rev. Lett. **61**, 1537 (1988).
- [17] B.T. Cleveland *et al.*, Nucl. Phys. B (Proc. Suppl.) **38**, 47 (1995); GALLEX collaboration, W. Hampel *et al.*, Phys. Lett. **B388**, 384 (1996); SAGE collaboration, J.N. Abdurashitov *et al.*, Phys. Rev. Lett. **77**, 4708 (1996); Kamiokande collaboration, Y. Fukuda *et al.*, Phys. Rev. Lett. **77**, 1683 (1996); Super-Kamiokande collaboration, Y. Fukuda *et al.*, Phys. Rev. Lett. **82**, 2430 (1999); Phys. Rev. Lett. **82**, 1810 (1999).
- [18] J.N. Bahcall, S. Basu, and M.H. Pinsonneault, Phys. Lett. **B 433**, 1 (1998), and references therein.

- [19] E. Church et al. (BooNE Collab.), “A letter of intent for an experiment to measure $\nu_\mu \rightarrow \nu_e$ oscillations and ν_μ at the Fermilab Booster”, May 16, 1997, unpublished.
- [20] Z. Maki, M. Nakagawa, and S. Sakata, Prog. Theor. Phys. **28**, 870 (1962).
- [21] L. Wolfenstein, Phys. Rev. **D17**, 2369 (1978).
- [22] V. Barger, S. Pakvasa, R.J.N. Phillips, and K. Whisnant, Phys. Rev. **D22**, 2718 (1980).
- [23] P. Langacker, J.P. Leveille, and J. Sheiman, Phys. Rev. **D 27**, 1228 (1983).
- [24] S.P. Mikheyev and A. Smirnov, Yad. Fiz. **42**, 1441 (1985) [Sov. J. Nucl. Phys. 42, 913 (1986)].
- [25] R. Bernstein and S. Parke, Phys. Rev. **D44**, 2069 (1991).
- [26] P. Lipari, hep-ph/9903481; E. Akhmedov, P. Lipari, and M. Lusignoli, Phys. Lett. **B300**, 128 (1993); P. Lipari and M. Lusignoli, Phys. Rev. **D58**, 073005 (1998); E. Akhmedov, A. Dighe, P. Lipari, and A.Yu. Smirnov, Nucl. Phys. **B542**, 3 (1999); E.K. Akhmedov, Nucl. Phys. **B538**, 25 (1998).
- [27] S.T. Petcov, Phys. Lett. **B434**, 321 (1998); M.V. Chizhov, M. Maris, and S.T. Petcov, hep-ph/9810501; M.V. Chizhov and S.T. Petcov, hep-ph/9903424; S.T. Petcov, hep-ph/9910335.
- [28] H.W. Zaglauer and K.H. Schwarzer, Z. Phys. **C40**, 273 (1988); Q. Liu, S. Mikheyev, and A.Yu. Smirnov, Phys. Lett. **B440**, 319 (1998); P.I. Krastev, Nuovo Cimento A **103**, 361 (1990).
- [29] J. Pruet and G.M. Fuller, astro-ph/9904023.
- [30] J. Pantaleone, Phys. Rev. **D49**, 2152 (1994); Phys. Rev. Lett. **81**, 5060 (1998).
- [31] J. Arafune, J. Sato, Phys. Rev. **D55**, 1653 (1997); J. Arafune, M. Koike and J. Sato, Phys. Rev. **D56**, 3093 (1997); M. Tanimoto, Prog. Theor. Phys. **97**, 901 (1997); H. Minakata and H. Nunokawa, Phys. Lett. **B413**, 369 (1997); H. Minakata and H. Nunokawa, Phys. Rev. **D57**, 4403 (1998); M. Koike and J. Sato, hep-ph/9909469; M. Koike and J. Sato, hep-ph/9911258.
- [32] I. Mocioiu and R. Shrock, hep-ph/9910554; T. Ohlsson and H. Snellman, hep-ph/9910546; A. Romanino, hep-ph/9909425.
- [33] Parameters of the Preliminary Reference Earth Model are given by A. Dziewonski, Earth Structure, Global, in “The Encyclopedia of Solid Earth Geophysics”, ed. by D.E. James, (Van Nostrand Reinhold, New York, 1989) p. 331; also see R. Gandhi, C. Quigg, M. Hall Reno, and I. Sarcevic, Astroparticle Physics **5**, 81 (1996).
- [34] V. Barger, K. Whisnant, R.J.N. Phillips, Phys. Rev. Lett. **45**, 2084 (1980)
- [35] R. Forty, hep-ex/9910061.
- [36] M.C. Gonzalez-Garcia, P.C. de Holanda, C. Peña-Garay, and J.W.F. Valle, hep-ph/9906469; J.N. Bahcall, P. Krastev, and A.Yu. Smirnov, hep-ph/9905220; J.N. Bahcall, P. Krastev, and A.Yu. Smirnov, Phys. Rev. **D58**, 096016 (1998); R. Barbieri, L.J. Hall, D. Smith, A. Strumia, and N. Weiner, JHEP 9812, 017 (1998); N. Hata and P. Langacker, Phys. Rev. **D56**, 6107 (1997).
- [37] The effects of the subleading oscillation scale in atmospheric neutrino experiments are discussed in O.L.G. Peres and A.Yu. Smirnov, Phys. Lett. **B456**, 204 (1999), hep-ph/9902312.
- [38] J.J. Gomez Cadenas, F. Dydak, A. C. Villanueva, presentation at the neutrino factory workshop, Lyon, 1999.

TABLES

TABLE I. Some candidate neutrino factory accelerator sites and long-baseline detector sites.

| Targets | Sources | | | | | | | | | | | |
|------------|----------|-----------------------------|------------------------|----------|-----------------------------|------------------------|----------|-----------------------------|------------------------|----------|-----------------------------|------------------------|
| | FNAL | | | BNL | | | CERN | | | KEK | | |
| | L (km) | $\langle Y_{e\rho} \rangle$ | dip angle ($^\circ$) | L (km) | $\langle Y_{e\rho} \rangle$ | dip angle ($^\circ$) | L (km) | $\langle Y_{e\rho} \rangle$ | dip angle ($^\circ$) | L (km) | $\langle Y_{e\rho} \rangle$ | dip angle ($^\circ$) |
| MINOS | 732 | 1.67 | 3.3 | 1715 | 1.67 | 7.7 | 6596 | 2.01 | 31 | 8559 | 2.20 | 42 |
| BNL | 1289 | 1.67 | 5.8 | | | | 5921 | 1.91 | 28 | 9607 | 2.31 | 49 |
| SLAC | 2913 | 1.67 | 13 | 4513 | 1.69 | 19 | 8590 | 2.20 | 42 | 7720 | 2.12 | 37 |
| Gran Sasso | 7332 | 2.09 | 35 | 6565 | 2.00 | 31 | 743 | 1.67 | 3.3 | 8844 | 2.23 | 44 |
| Kamioka | 9165 | 2.26 | 46 | 9667 | 2.31 | 49 | 8774 | 2.22 | 44 | 252 | 1.67 | 1.1 |

TABLE II. Signatures for various oscillation channels when negative muons are stored.

| signature | oscillation | produced | detected |
|------------------------------|--|----------|----------|
| | | lepton | muon |
| ν_μ -survival | $\nu_\mu \rightarrow \nu_\mu$ | μ^- | μ^- |
| ν_τ -appearance | $\nu_\mu \rightarrow \nu_\tau$ | τ^- | μ^- |
| $\bar{\nu}_\mu$ -appearance | $\bar{\nu}_e \rightarrow \bar{\nu}_\mu$ | μ^+ | μ^+ |
| $\bar{\nu}_\tau$ -appearance | $\bar{\nu}_e \rightarrow \bar{\nu}_\tau$ | τ^+ | μ^+ |

TABLE III. Predicted event rates in a 10 kt detector per 2×10^{20} muon decays, with the oscillation parameters specified by Eq. (43).

| | sign of δm_{32}^2 | $E_{\mu+}$ (GeV) | | | $E_{\mu-}$ (GeV) | | |
|-----------------------------------|------------------------------|------------------|---------|-----------|------------------|---------|-----------|
| | | 10 | 30 | 50 | 10 | 30 | 50 |
| $L = 732$ km | | | | | | | |
| ν_{μ} (no osc) | | 14,300 | 382,000 | 1,780,000 | 29,000 | 772,000 | 3,560,000 |
| $\nu_{\mu} \rightarrow \nu_{\mu}$ | + | 11,200 | 372,000 | 1,760,000 | 22,800 | 750,000 | 3,520,000 |
| | - | 11,200 | 372,000 | 1,760,000 | 22,900 | 751,000 | 3,530,000 |
| ν_e (no osc) | | 24,200 | 656,000 | 3,050,000 | 12,400 | 329,000 | 1,520,000 |
| $\nu_e \rightarrow \nu_{\mu}$ | + | 158 | 404 | 1000 | 69.4 | 276 | 486 |
| | - | 106 | 410 | 718 | 65.2 | 223 | 380 |
| $L = 2800$ km | | | | | | | |
| ν_{μ} (no osc) | | 1140 | 27,500 | 123,000 | 2200 | 52,500 | 244,000 |
| $\nu_{\mu} \rightarrow \nu_{\mu}$ | + | 168 | 18,800 | 107,000 | 274 | 36,000 | 212,000 |
| | - | 164 | 18,900 | 107,000 | 274 | 36,200 | 212,000 |
| ν_e (no osc) | | 1400 | 43,300 | 211,000 | 900 | 22,600 | 102,000 |
| $\nu_e \rightarrow \nu_{\mu}$ | + | 54 | 486 | 894 | 4 | 88 | 224 |
| | - | 3.4 | 130 | 338 | 36 | 214 | 356 |
| $L = 7332$ km | | | | | | | |
| ν_{μ} (no osc) | | 152 | 3880 | 17,500 | 294 | 7660 | 35,600 |
| $\nu_{\mu} \rightarrow \nu_{\mu}$ | + | 84 | 592 | 7220 | 130 | 1040 | 14,900 |
| | - | 72 | 558 | 7340 | 160 | 1130 | 15,000 |
| ν_e (no osc) | | 21.8 | 6680 | 30,500 | 120 | 3300 | 15,200 |
| $\nu_e \rightarrow \nu_{\mu}$ | + | 21.6 | 274 | 300 | 0.66 | 9 | 19.8 |
| | - | 1.14 | 18 | 38 | 12.8 | 132 | 145 |

TABLE IV. Predicted event rates in a 10 kt detector per 2×10^{20} muon decays, with $\sin^2 2\theta_{13} = 0.004$ and the other oscillation parameters specified by Eq. (43).

| | sign of δm_{32}^2 | $E_{\mu+}$ (GeV) | | | $E_{\mu-}$ (GeV) | | |
|-------------------------------|------------------------------|------------------|---------|-----------|------------------|---------|-----------|
| | | 10 | 30 | 50 | 10 | 30 | 50 |
| $L = 732$ km | | | | | | | |
| ν_μ (no osc) | | 14,300 | 382,000 | 1,780,000 | 29,000 | 772,000 | 3,560,000 |
| $\nu_\mu \rightarrow \nu_\mu$ | + | 11,200 | 372,000 | 1,760,000 | 22,800 | 750,000 | 3,520,000 |
| | - | 11,200 | 372,000 | 1,760,000 | 22,900 | 751,000 | 3,530,000 |
| ν_e (no osc) | | 24,200 | 656,000 | 3,050,000 | 12,400 | 329,000 | 1,520,000 |
| $\nu_e \rightarrow \nu_\mu$ | + | 19.4 | 73.6 | 127 | 8.6 | 35.2 | 61.8 |
| | - | 8.4 | 30.2 | 52.2 | 5.34 | 16.6 | 27.8 |
| $L = 2800$ km | | | | | | | |
| ν_μ (no osc) | | 1140 | 27,500 | 123,000 | 2200 | 52,500 | 244,000 |
| $\nu_\mu \rightarrow \nu_\mu$ | + | 168 | 18,800 | 107,000 | 276 | 35,900 | 212,000 |
| | - | 166 | 18,900 | 107,000 | 274 | 36,200 | 212,000 |
| ν_e (no osc) | | 1400 | 43,300 | 211,000 | 900 | 22,600 | 102,000 |
| $\nu_e \rightarrow \nu_\mu$ | + | 5.2 | 56.4 | 108 | 0.82 | 11.6 | 29 |
| | - | 0.64 | 10 | 24.6 | 4.4 | 19.2 | 29.6 |
| $L = 7332$ km | | | | | | | |
| ν_μ (no osc) | | 152 | 3800 | 17,500 | 294 | 7660 | 35,600 |
| $\nu_\mu \rightarrow \nu_\mu$ | + | 84 | 586 | 7140 | 152 | 1100 | 14,600 |
| | - | 84 | 586 | 7220 | 158 | 1200 | 15,000 |
| ν_e (no osc) | | 218 | 6680 | 30,500 | 120 | 3300 | 15,200 |
| $\nu_e \rightarrow \nu_\mu$ | + | 2.58 | 30.2 | 32.8 | 0.066 | 0.89 | 1.98 |
| | - | 0.112 | 1.77 | 3.8 | 1.52 | 14.6 | 144 |

TABLE V. Statistical precision in determining $\sin^2 2\theta_{23}$ and δm_{32}^2 if $\sin^2 2\theta_{23} = 1.0$ and $\delta m_{32}^2 = 3.5 \times 10^{-3} \text{eV}^2$. Fit results are tabulated for various muon storage ring energies and baselines.

| E_μ (GeV) | L (km) | Events fitted | Fitted energy range (GeV) | $\sin^2 2\theta_{23}$ % error | δm_{32}^2 % error |
|---------------|----------|---------------|------------------------------|----------------------------------|------------------------------|
| 10 | 732 | 847 | 0-4 | 7.6 | 6.7 |
| 10 | 2800 | 284 | 0-10 | 1.1 | 2.4 |
| 10 | 7332 | 126 | 0-12 | 13 | 6.3 |
| 30 | 732 | 3984 | 0-12 | 14 | 8.9 |
| 30 | 2800 | 623 | 0-12 | 2.0 | 3.2 |
| 30 | 7332 | 655 | 0-25 | 0.57 | 1.2 |
| 50 | 732 | 1573 | 0-12 | 17 | 12 |
| 50 | 2800 | 169 | 0-10 | 1.8 | 4.9 |
| 50 | 7332 | 834 | 0-28 | 0.64 | 1.4 |

TABLE VI. Summary of sensitivity versus baseline and stored muon energy.

| L (km) | E_μ (GeV) | Survival | | Appearance | | |
|----------|---------------|---|---|--|---|--|
| | | $\sin^2 2\theta_{23}$ statistical precision | δm_{32}^2 statistical precision | $\sin^2 2\theta_{13}$ 10 Event sensitivity | $\sin^2 2\theta_{13}$ 3σ sign δm^2 | matter + δm_{21}^2 effects |
| 732 | 10 | 7.6% | 6.7% | 0.002 | >0.1 | large |
| 732 | 30 | 14% | 8.9% | 0.0005 | 0.1 | large |
| 732 | 50 | 17% | 12% | 0.0003 | > 0.1 | large |
| 2800 | 10 | 1.1% | 2.4% | 0.008 | 0.1 | moderate |
| 2800 | 30 | 2.0% | 3.2% | 0.0007 | 0.005 | moderate |
| 2800 | 50 | 1.8% | 4.9% | 0.0004 | 0.003 | moderate |
| 7332 | 10 | 13% | 6.3% | 0.02 | >0.1 | negligible |
| 7332 | 30 | 0.57% | 1.2% | 0.001 | 0.04 | negligible |
| 7332 | 50 | 0.64% | 1.4% | 0.002 | 0.02 | negligible |

FIGURES

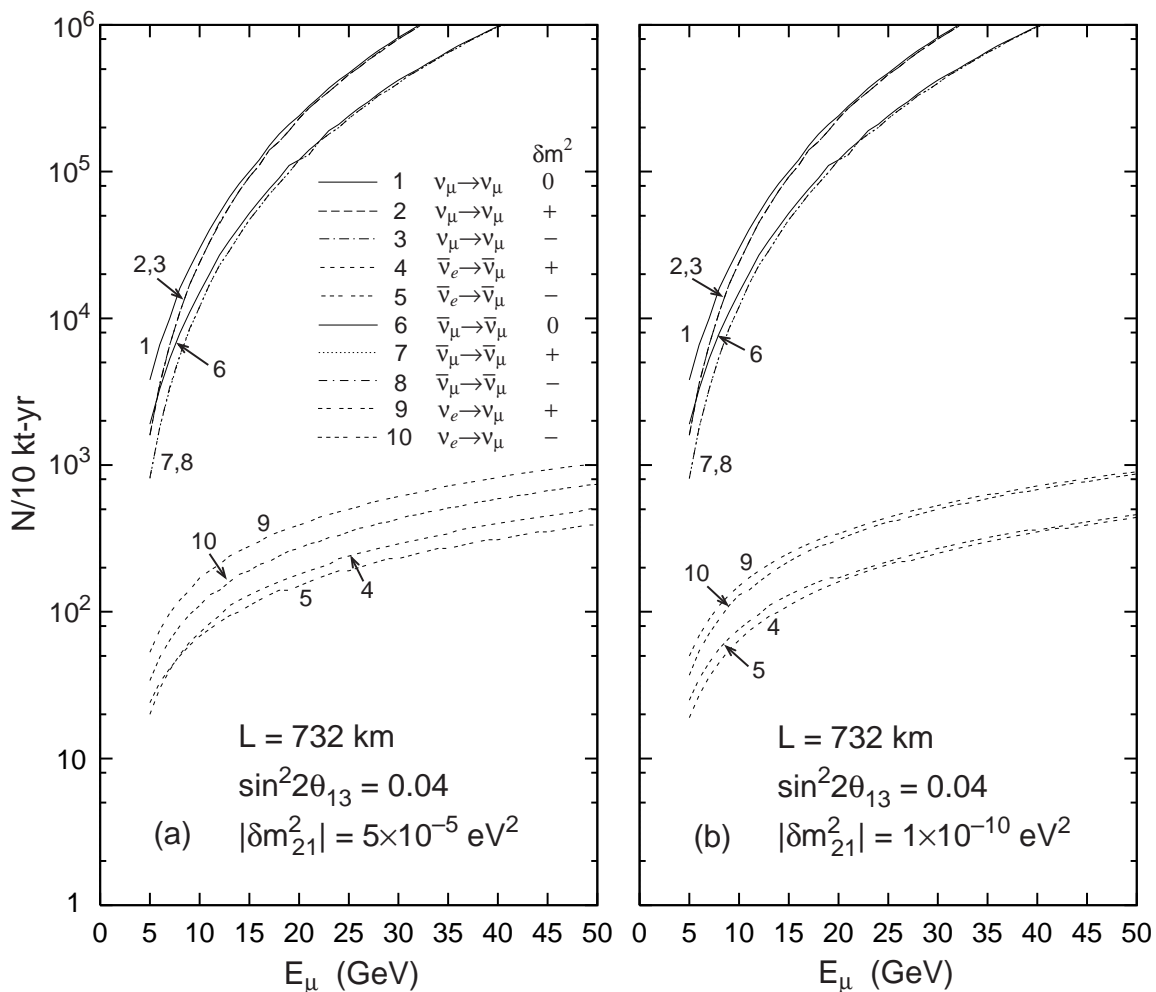


FIG. 1. Muon survival and appearance events per 10 kt-yr versus muon energy at $L = 732$ km, assuming 2×10^{20} muon decays per year. The oscillation parameters are those given in Eq. (43) and (a) $\delta m_{21}^2 = 5 \times 10^{-5} \text{ eV}^2$ and (b) $\delta m_{21}^2 \sim 1 \times 10^{-10} \text{ eV}^2$. The upper (lower) solid curve shows the rates without oscillations for neutrinos (antineutrinos). For the rates with oscillations, the results are shown for both signs of δm_{32}^2 .

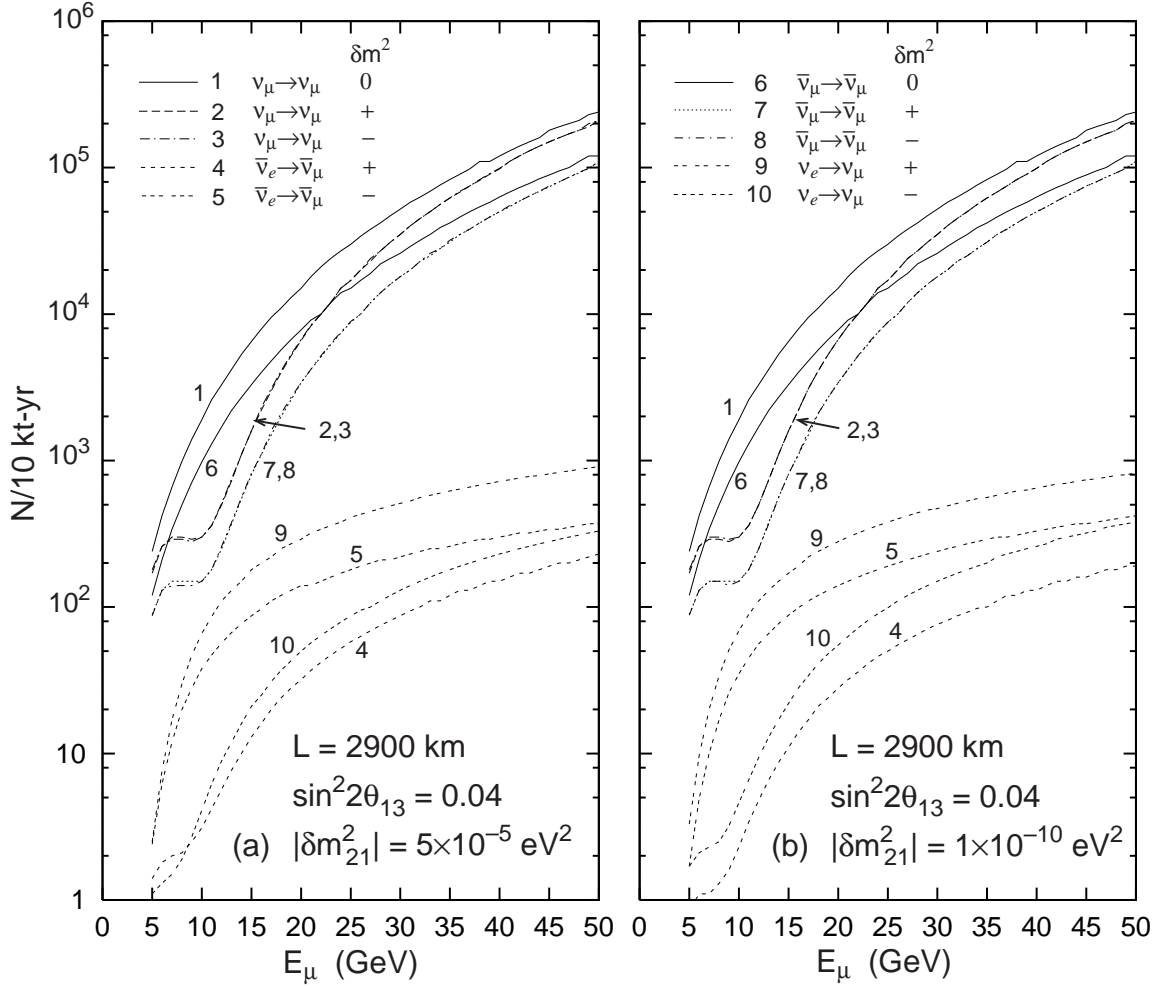


FIG. 2. Same as Fig. 1 except $L = 2900 \text{ km}$.

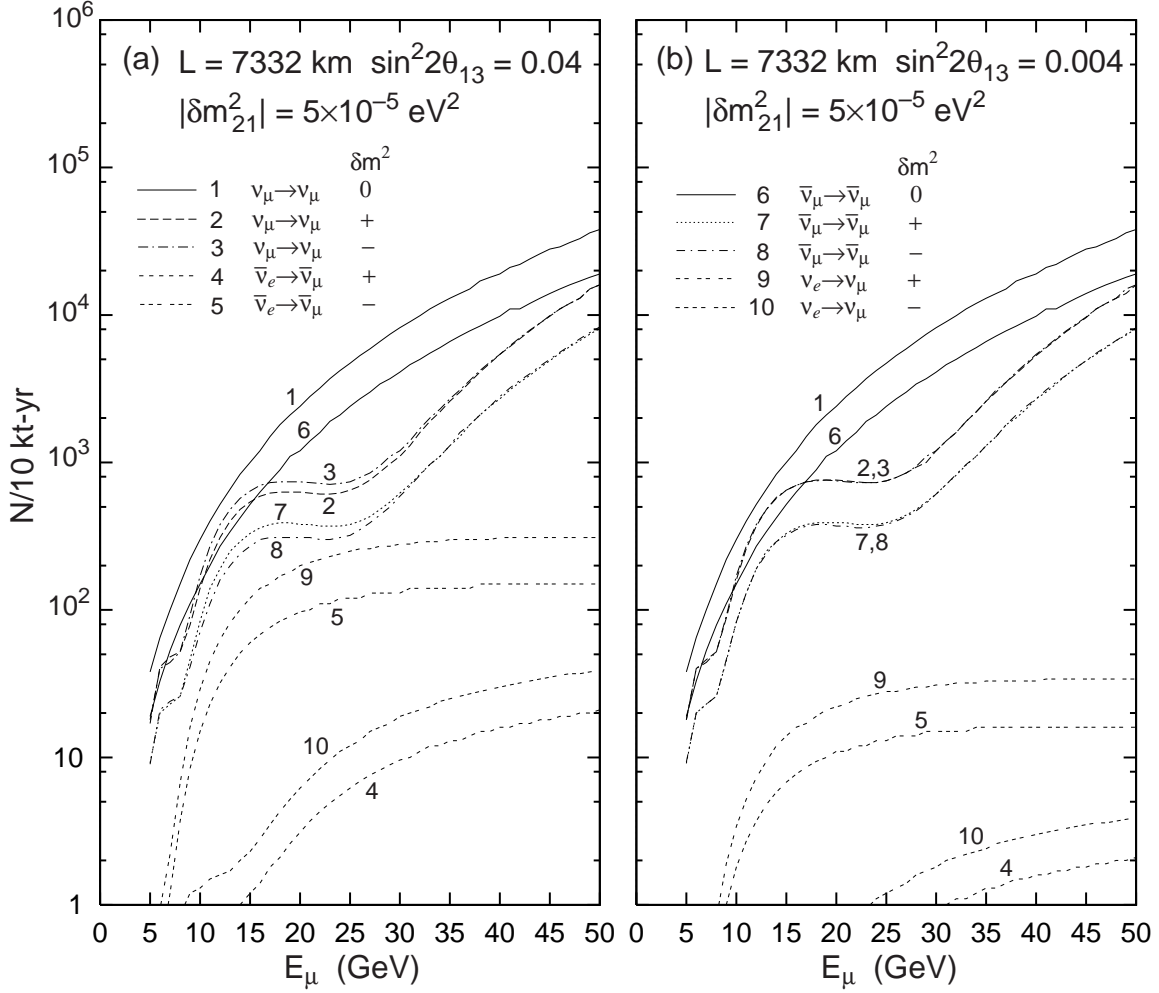


FIG. 3. Same as Fig. 1 except $L = 7332 \text{ km}$, $\delta m_{21}^2 = 5 \times 10^{-5} \text{ eV}^2$, and (a) $\sin^2 2\theta_{13} = 0.04$ and (b) $\sin^2 2\theta_{13} = 0.004$.

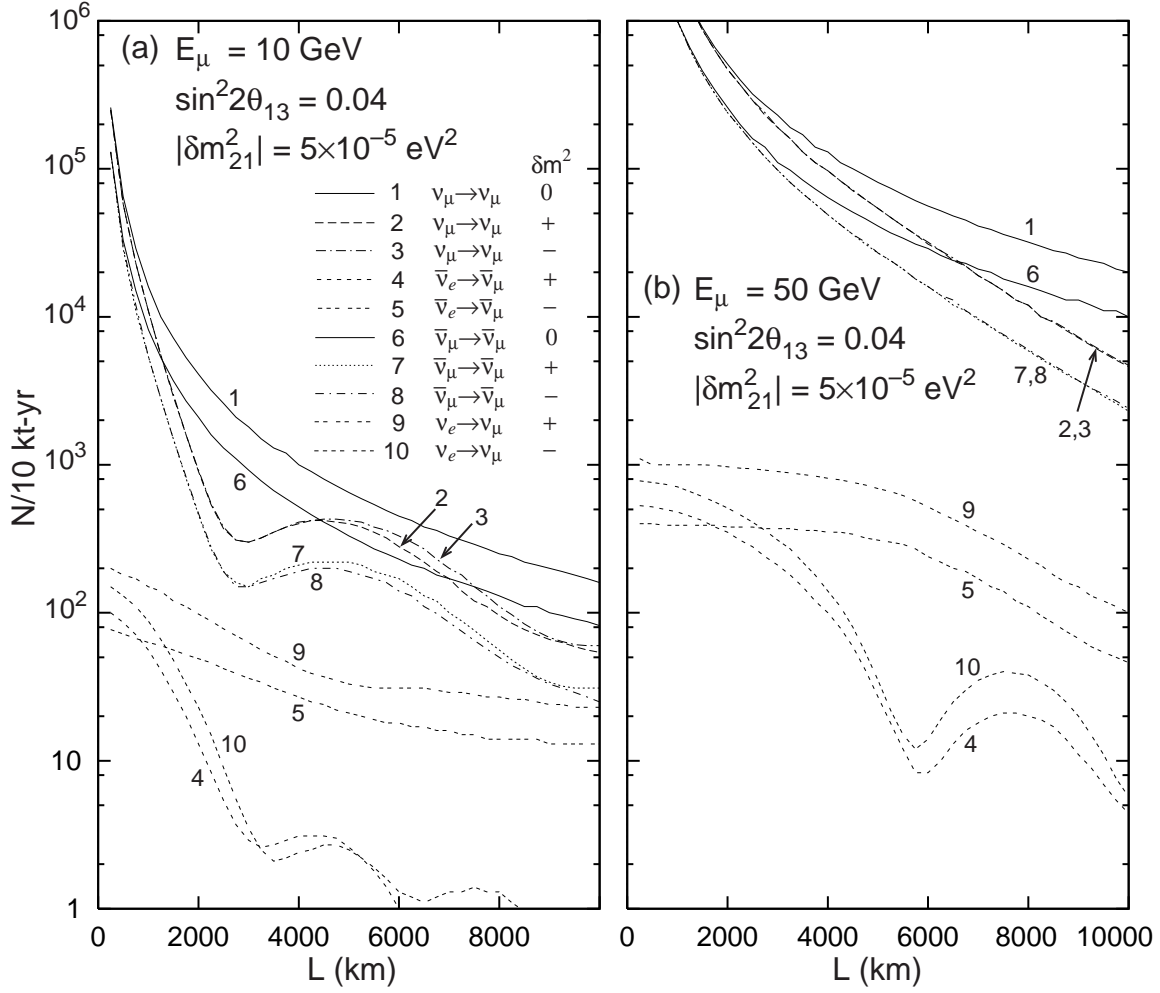


FIG. 4. Muon survival and appearance rates per 10 kt-yr versus detector distance for (a) $E_\mu = 10 \text{ GeV}$ and (b) $E_\mu = 50 \text{ GeV}$. The oscillation parameters used are given in Eq. (43).

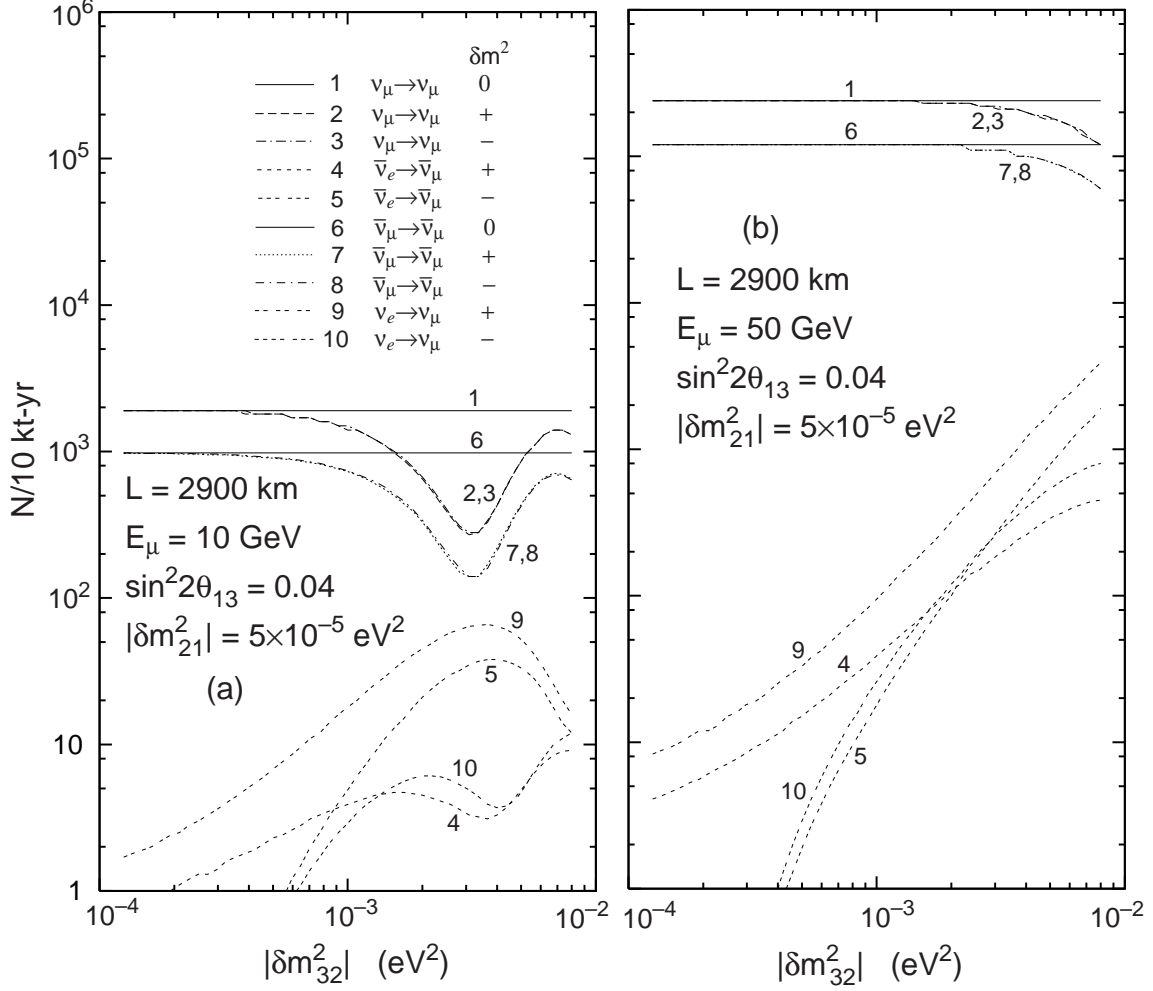


FIG. 5. Muon survival and appearance rates per 10 kt-yr versus $|\delta m_{32}^2|$ at $L = 2900 \text{ km}$ for (a) $E_\mu = 10 \text{ GeV}$ and (b) $E_\mu = 50 \text{ GeV}$. The other oscillation parameters are given in Eq. (43).

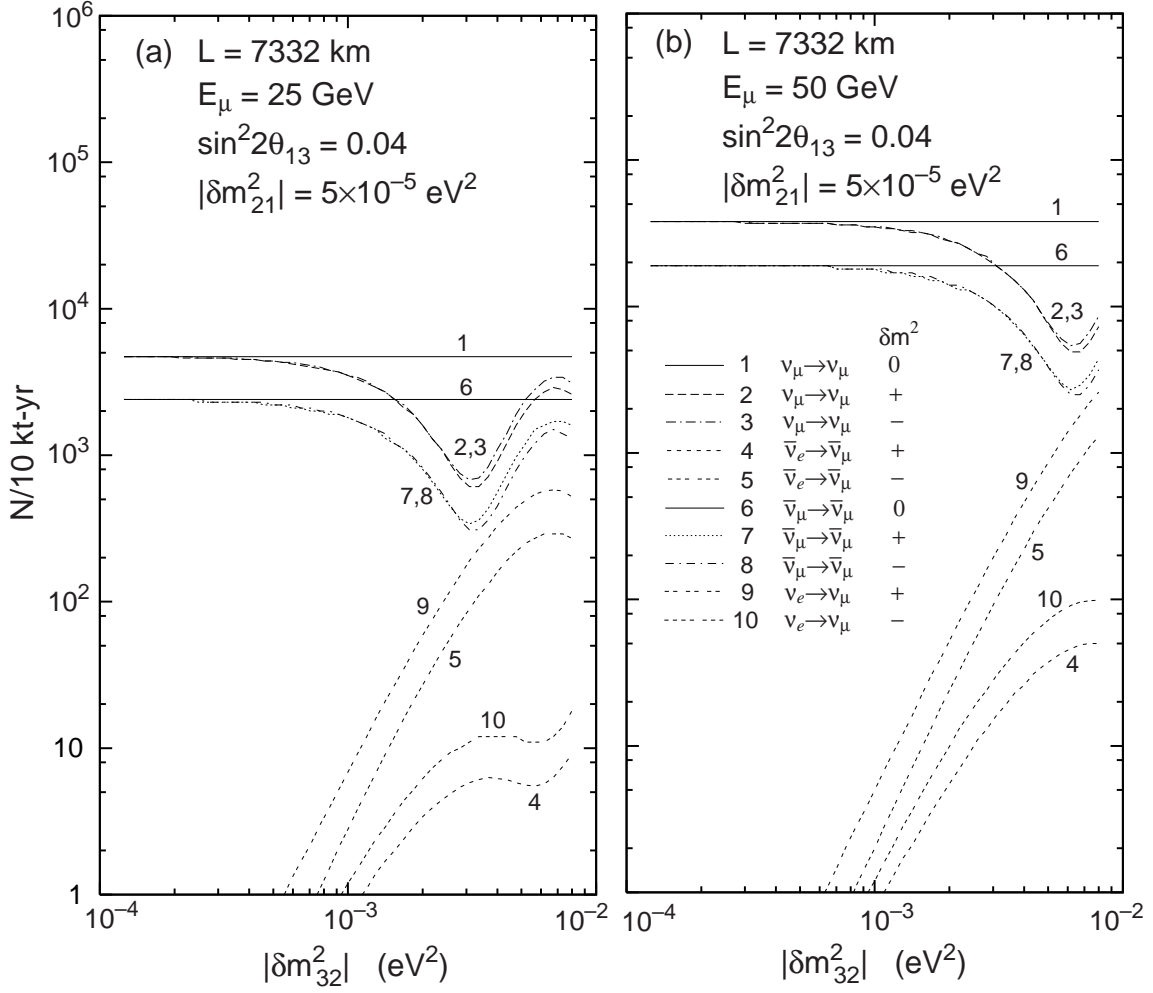


FIG. 6. Same as Fig. 5 except $L = 7332$ km.

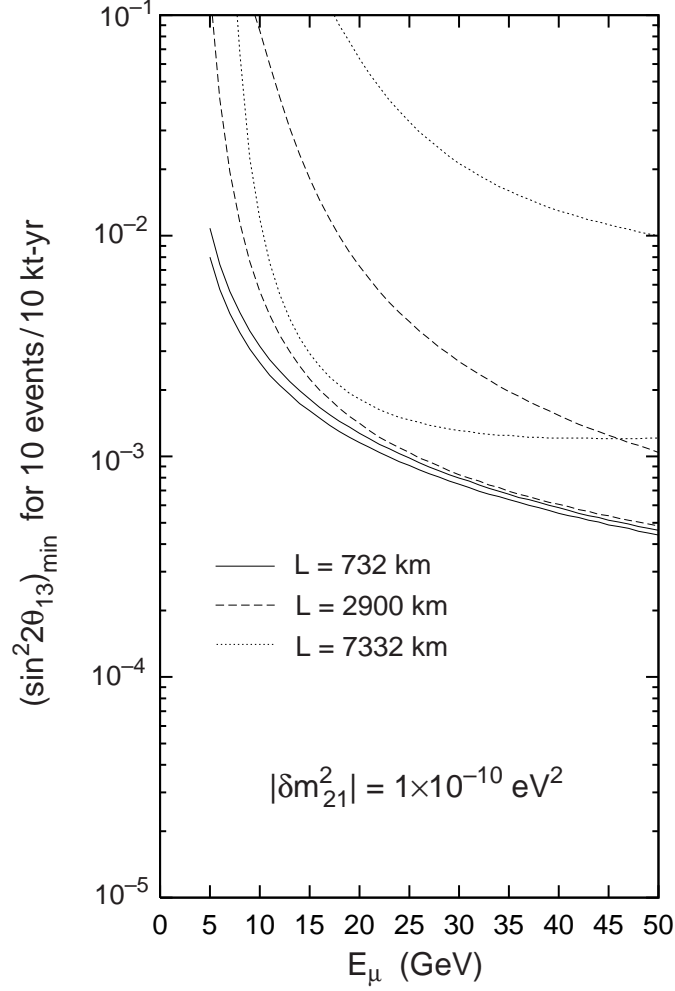


FIG. 7. Minimum value of $\sin^2 2\theta_{13}$ that gives 10 $\nu_e \rightarrow \nu_\mu$ appearance events in a 10 kt detector with a source of 2×10^{20} muon decays/yr, for $L = 732$ km (solid curves), 2900 km (dashed curves), and 7332 km (dotted curves). The oscillation parameters are given in Eq. (43) and $\delta m_{21}^2 \sim 1 \times 10^{-10} \text{ eV}^2$. The lower (upper) curve in each case is the result for $\delta m_{32}^2 > 0$ ($\delta m_{32}^2 < 0$). The corresponding curves for $\bar{\nu}_e \rightarrow \bar{\nu}_\mu$ appearance are given approximately by interchanging the upper and lower curves and dividing by a factor of 2.

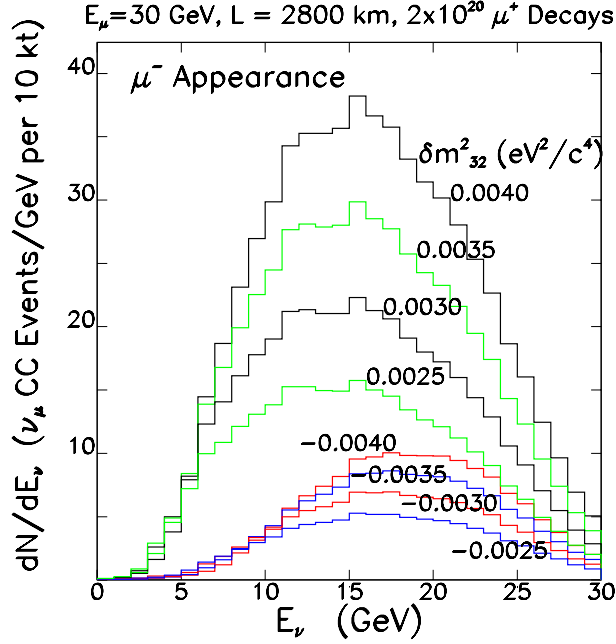


FIG. 8. Predicted measured energy distributions for CC events tagged by a wrong-sign (negative) muon from $\nu_e \rightarrow \nu_\mu$ oscillations, shown for various δm_{32}^2 , as labelled. The predictions correspond to 2×10^{20} decays, $E_\mu = 30$ GeV, $L = 2800$ km, with the values for $\delta m_{12}^2, s_{13}, s_{23}, s_{12}$, and δ given in Eq. (43).

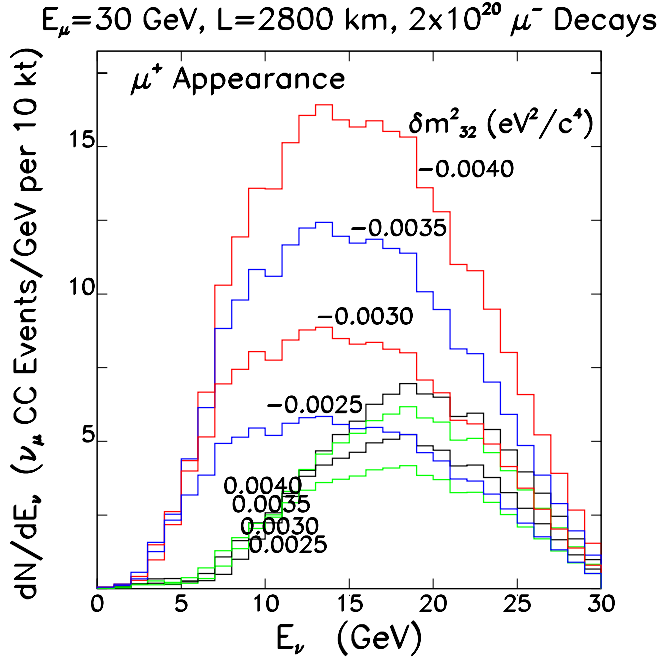


FIG. 9. Predicted measured energy distributions for CC events tagged by a wrong-sign (positive) muon from $\bar{\nu}_e \rightarrow \bar{\nu}_\mu$ oscillations, shown for various δm_{32}^2 , as labelled. The predictions correspond to 2×10^{20} decays, $E_\mu = 30$ GeV, $L = 2800$ km, with the values for $\delta m_{12}^2, s_{13}, s_{23}, s_{12}$, and δ given in Eq. (43).

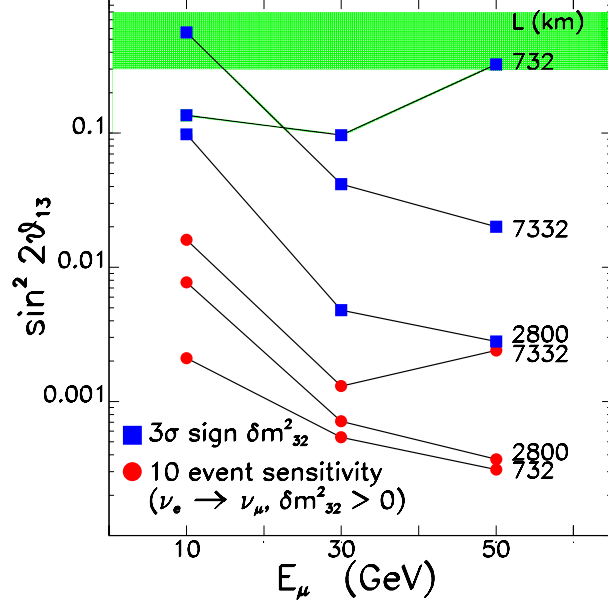


FIG. 10. The value of $\sin^2 2\theta_{13}$ that yields, in a 10 kt detector at $L = 2800$ km, (a) 10 events per $2 \times 10^{20} \mu^+$ decays (boxes), and (b) a three standard deviation determination of the sign of δm_{32}^2 when the wrong-sign muon event rates for $2 \times 10^{20} \mu^+$ decays are compared with the corresponding rates for $2 \times 10^{20} \mu^-$ decays (circles). The $\sin^2 2\theta_{13}$ sensitivity is shown versus E_μ and L (as labelled). The calculations assume the values for $|\delta m_{32}^2|$, δm_{12}^2 , s_{23} , s_{12} , δ given in Eq. (43). The shaded region is excluded by the existing data.

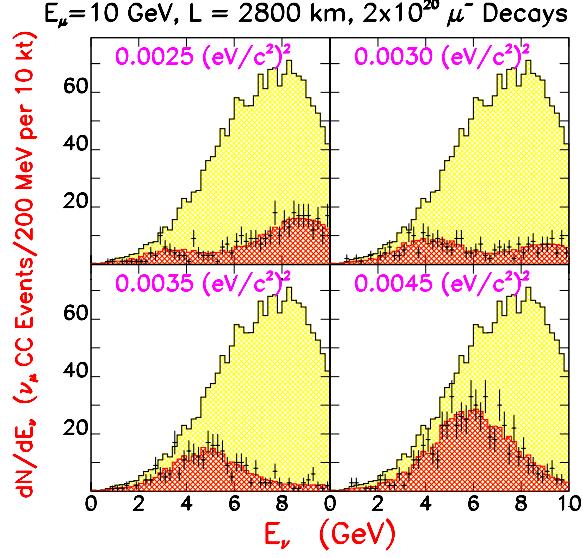


FIG. 11. Predicted measured energy distributions for CC $\nu_\mu \rightarrow \nu_\mu$ events shown for four different δm_{32}^2 (darkly shaded distributions) as labelled. The predictions correspond to 2×10^{20} decays, $E_\mu = 10 \text{ GeV}$, $L = 2800 \text{ km}$, with the values for $\delta m_{12}^2, s_{13}, s_{23}, s_{12}$, and δ given in Eq. (43). The predicted distribution has been used to generate a Monte Carlo dataset with the statistics corresponding to a 10 kt-yr dataset (points with error bars). The lightly shaded histograms show the predicted distributions in the absence of oscillations.

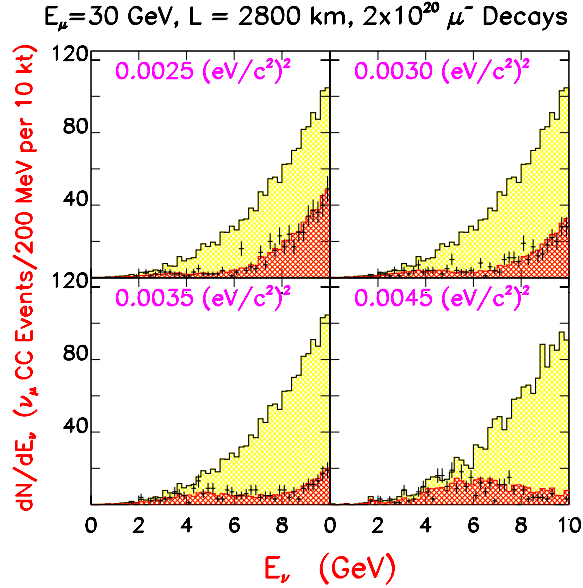


FIG. 12. Predicted measured energy distributions for CC $\nu_\mu \rightarrow \nu_\mu$ events shown for four different δm_{32}^2 (darkly shaded distributions) as labelled. The predictions correspond to 2×10^{20} decays, $E_\mu = 30 \text{ GeV}$, $L = 2800 \text{ km}$, with the values for $\delta m_{12}^2, s_{13}, s_{23}, s_{12}$, and δ given in Eq. (43). The predicted distribution has been used to generate a Monte Carlo dataset with the statistics corresponding to a 10 kt-yr dataset (points with error bars). The lightly shaded histograms show the predicted distributions in the absence of oscillations.

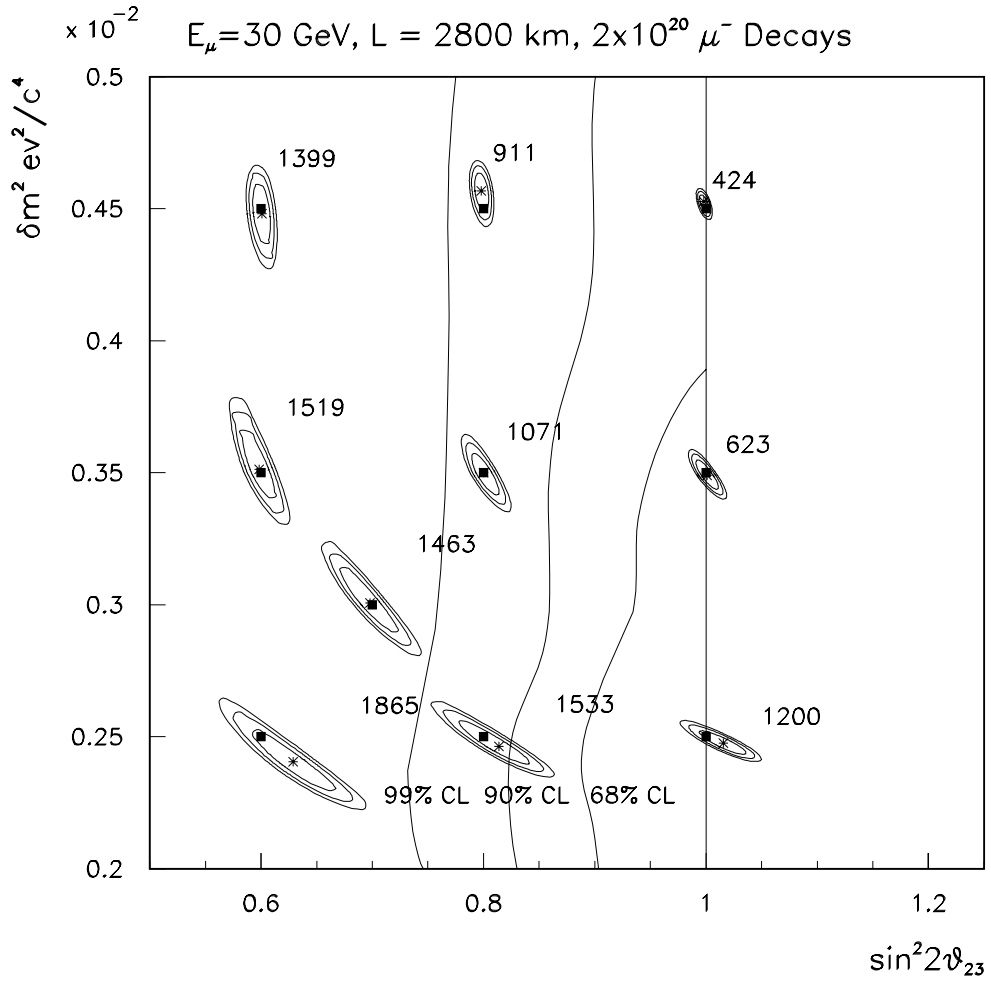


FIG. 13. Fit to muon neutrino survival distribution for $E_\mu = 30 \text{ GeV}$ and $L = 2800 \text{ km}$ for 10 pairs of $\sin^2 2\theta$, δm^2 values. For each fit, the 1σ , 2σ and 3σ contours are shown. The generated points are indicated by the dark rectangles and the fitted values by stars. The SuperK 68%, 90%, and 95% confidence levels are superimposed. Each point is labelled by the predicted number of signal events for that point.

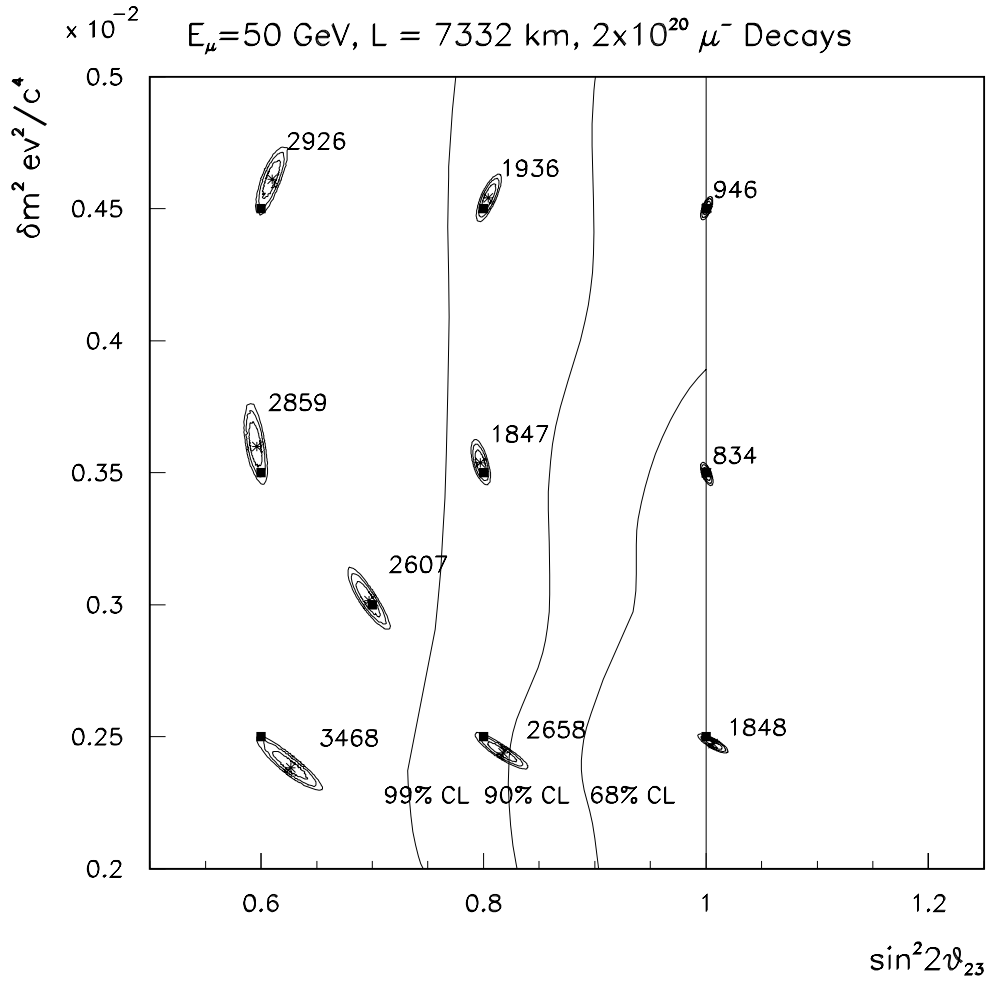


FIG. 14. Fit to muon neutrino survival distribution for $E_\mu = 50 \text{ GeV}$ and $L = 7332 \text{ km}$ for 10 pairs of $\sin^2 2\theta$, δm^2 values. For each fit, the 1σ , 2σ and 3σ contours are shown. The generated points are indicated by the dark rectangles and the fitted values by stars. The SuperK 68%, 90%, and 95% confidence levels are superimposed. Each point is labelled by the predicted number of signal events for that point.